

We are IntechOpen, the world's leading publisher of Open Access books Built by scientists, for scientists

6,900

Open access books available

186,000

International authors and editors

200M

Downloads

Our authors are among the

154

Countries delivered to

TOP 1%

most cited scientists

12.2%

Contributors from top 500 universities



WEB OF SCIENCE™

Selection of our books indexed in the Book Citation Index
in Web of Science™ Core Collection (BKCI)

Interested in publishing with us?
Contact book.department@intechopen.com

Numbers displayed above are based on latest data collected.
For more information visit www.intechopen.com



Tapered Optical Fibers – An Investigative Approach to the Helical and Liquid Crystal Types

P. K. Choudhury

Institute of Microengineering & Nanoelectronics (IMEN)

*Universiti Kebangsaan Malaysia, Bangi, Selangor
Malaysia*

1. Introduction

Optical waveguides find multifarious applications in integrated optical devices as well as various forms of communication systems. In order to get a good understanding of the optical features of waveguides, the basic requirement is to analyze the propagation characteristics of electromagnetic (EM) waves through the guide. In this context, the study of EM wave propagation through various types of optical fibers and waveguides has been greatly dealt with, which can be witnessed through the vast research reports by the relevant R&D community, as appeared in the literature. In this context, several forms of optical waveguides implementing different composite materials [1–6] and/or new forms of geometrical cross-sections [7–13] have been developed most of which are now widely recognized for their use in the fabrication of integrated optical circuits and in the laser beam technology. These include unconventional types of waveguide geometries too [3,13].

The study of EM wave propagation through conventional optical fibers does not involve much difficulty. Among the various types of fiber structures, fibers with tapers and flares have received considerable attention over the years because of their promising applicability in the area of fused fiber couplers [14–30]. These tapered optical fibers (TOFs) are of practical interest for the fabrication of *all-optical* components as these miniaturized optical components find enormous potential applications in the areas related to optical sensors as well as other in-line integrated optic applications where directional couplers and beam expanders are being used [31–34].

It is noteworthy that dielectric TOFs can be used with much efficiency in evanescent wave fiber-optic absorption sensors. This way, TOFs become one of the most promising means in high-speed transmission systems. Optically, the taper transitions transform the local fundamental mode from a core mode in the untapered fiber to a cladding mode in the taper waist – the basis of many of its *all-optical* applications including multiplexing and modulation. It is desirable for the transition to be as short as possible, allowing the resulting component to be compact and insensitive to the degradation of the environment.

Treatment of TOFs presents formidable mathematical difficulties, and therefore, a recourse has to be taken to a variety of approximate methods. In the present article, we

make a review of the different types of reported TOFs. Starting with the very fundamental form of TOF, which is the dielectric TOF, we venture into the investigations of their other complicated forms, viz. helical clad TOFs (or TOFs with twists) and the liquid crystal TOFs.

Fundamental studies on tapered guides include emphasis on optical fiber up-tapers for single-mode hardware applications and laser transmission evaluation. Among the various techniques, the implementation of split-step method would be one of the potential ways for the analytical treatment of a TOF, wherein the guide itself can be viewed in the analogy with a stack of large number of fibers of increasing (or decreasing) cross-sectional dimension with an end-to-end contact. The present article discusses the formulation of TOFs with regard to the various possible modes as it falls in the region of interest where one would require a suitable fiber design. In this context, the study of dispersion characteristics of fibers/waveguides has importance in the determination of their performance. Apart from that, the propagation of power also plays the determining role in selecting the suitability of the guide for specific applications.

Helical structures find useful applications in all low- and medium-power traveling wave tubes, the analyses of which generally include waveguides under slow-wave structures with conducting sheath and tape helices [35]. Such a concept can be implemented in the case of optical fibers taking into consideration the case of sheath helix windings [36]. A closer look at the dispersion behavior of such TOFs would be rather interesting as the helix pitch angle itself plays a major role to control the dispersion behavior of the guide. The present article covers all these issues corresponding to particular values of the helix pitch angle – windings perpendicular and parallel to the direction of EM wave propagation. Under the assumption of a small variation of the core radius in the longitudinal direction, it is demonstrated that the helix pitch greatly affects the propagation through the guide, making thereby the angle of pitch as one of the dominant controlling parameters, so far as the fiber design is considered. This is further verified through the comparison of results with those obtained for dielectric TOFs without helical windings.

Liquid crystal fibers (LCFs) exhibit polarization anisotropy, which make them of much technological interest and useful for many optical applications [5,37–39]. It is interesting to note that the macroscopic optical properties of liquid crystals can be manipulated by suitably applying the external electrical fields [40]. This feature essentially remains of promising use in optical sensing. Radial and azimuthal would be two different types of anisotropy, which LCFs may possess. The present article also incorporates a section that reports the study of an amalgamation of the taper structure and the clad anisotropy; it is demonstrated that the LCF structure supports enhanced power in the outer clad region – a much desirable characteristics for optical sensing and field coupling devices.

The arrangement of the present article is made in this way – the entire volume is divided into five different sections. Apart from the ongoing Section 1, we described the dielectric TOFs in Section 2, where the attempts are made to discuss the dispersion relations of dielectric TOFs along with the sustained transmission of power. In Section 3, twisted TOFs are described where the twists are introduced through the helical wraps at the core/clad interface. In this section, the effects on the dispersion relations due to the angle of twists are emphasized. Section 4 incorporates the study of LCFs where the effects of introducing a radially anisotropic layer at the outermost TOF region are investigated. The

transmission of power through such LCFs is also touched upon. A concluding remark is presented in Section 5 that wraps the themes of the results obtained corresponding to the different types of TOFs.

2. Dielectric tapered fibers

The analytical treatment of TOFs remains much complicated. In order to deal with the problem, among the available techniques, the split-step method is the one which can be utilized with much accuracy. In this method, a TOF can be viewed in the analogy with a stack of large number of tiny sections of fibers with increasing (or decreasing) cross-sectional dimension with an end-to-end arrangement.

Fundamental studies of TOFs have been appeared in the literature [31–34]. However, the dispersion characteristics of TOFs are less discussed. In this section, we present the formulation of TOFs in respect of possible sustained modes as it remains important to work on the fiber design based on the requirements. Further, the study of dispersion characteristics of fibers/waveguides is much important in the determination of their performance. In the following sub-sections, using Maxwell's field equations, we make an attempt to present the dispersion characteristics and cutoff situations of a dielectric TOF with the special mention of the dispersion curves corresponding to different modes. The features of such TOFs in respect of the transmission of power are also described emphasizing the power confinement factor of the guide.

2.1 Theoretical development

To deduce the exact field solutions for dielectric TOFs, the full set of Maxwell's equations resulting in the vector-wave equation for the system must be implemented. Fig. 1 illustrates the transverse view of a step-index dielectric TOF where the core/clad regions have refractive index (RI) values as n_1 and n_2 , respectively. For simplicity, we consider the clad section as infinitely extended. We use the cylindrical polar coordinate system (ρ, ϕ, z) for the analysis with the z -axis as the direction of propagation. We consider fiber with a linearly tapered core having varying taper radius ρ represented by the function

$$\rho = \begin{cases} a_0, & z \leq z_1 \\ a_0 \left[1 + (\alpha - 1) \sin^2 \left\{ \frac{\pi}{2} \left(\frac{z - z_1}{z_2 - z_1} \right) \right\} \right], & z_1 < z < z_2 \\ \alpha a_0, & z \geq z_2 \end{cases} \quad (1)$$

In eq. (1) α is the overall geometrical magnification factor, a_0 is the fiber core radius at the input end and $(z_2 - z_1)$ is the length of the taper [41]. Eq. (1) represents the function to determine the size of the varying radius along the tapered core. The function ρ and its derivative remain continuous at $z = z_1$ and $z = z_2$. The region $z < z_1$ corresponds to the fiber pigtail whereas $z > z_2$ to the expanded cylindrical section (straight tip) following the taper. For the analytical treatment, we follow the method reported earlier by Amitay *et al.* [41], i.e. $z_1 = 0$.

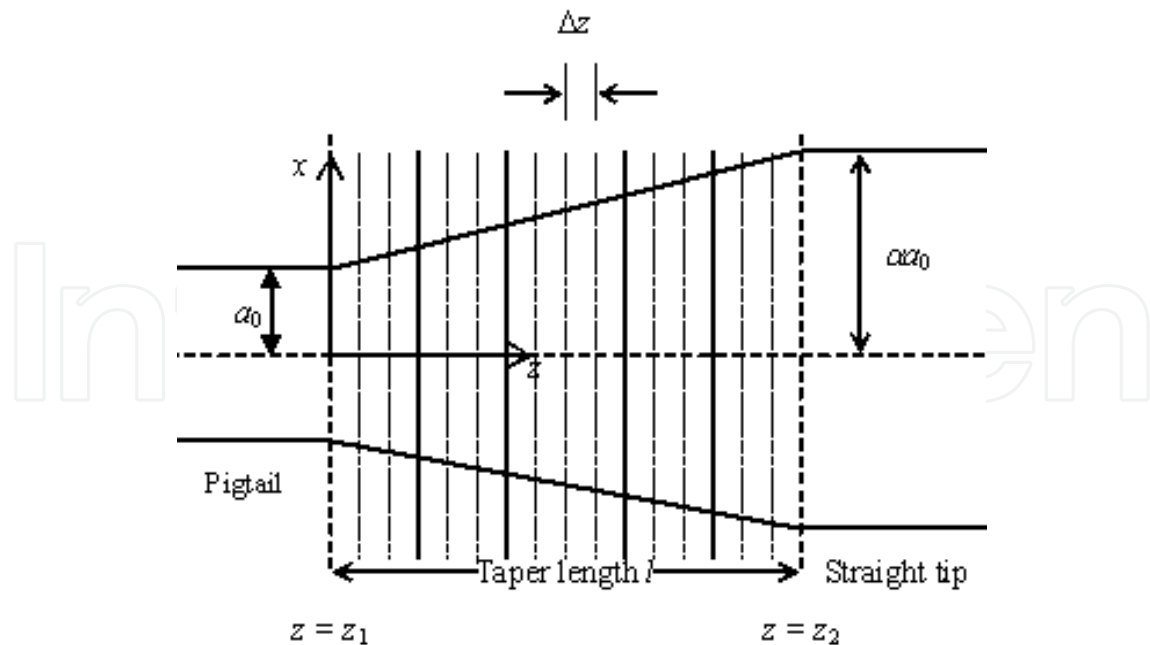


Fig. 1. Transverse view of dielectric TOF.

In another way, the linearly tapered geometrical profile of the fiber core may also be defined by

$$\rho(z) = \rho_i - \frac{z}{l}(\rho_i - \rho_o), \quad (2)$$

where $\rho = \rho_i$ and $\rho = \rho_o$ represent the radius of the input and the output ends, respectively, of the tapered fiber, and l is the length of the taper.

We assume that the core/clad regions are made of linear, homogeneous, isotropic and non-magnetic (i.e. $\mu_1 = \mu_2 \cong \mu_0$, the free-space permeability) materials, and they have the permittivity as ε_1 and ε_2 , respectively. The time t -harmonic and the axis z -harmonic electric and magnetic fields will have their functional dependences of the form

$$\mathbf{E} = \mathbf{E}_0(\rho) e^{j\nu\phi} e^{j(\omega t - \beta z)}, \quad (3a)$$

$$\mathbf{H} = \mathbf{H}_0(\rho) e^{j\nu\phi} e^{j(\omega t - \beta z)} \quad (3b)$$

with ω as the angular frequency, β as the propagation constant in the axial direction and ν as the azimuthal periodicity. In the present case, β is no longer a constant owing to the gradual variation of the cross-sectional dimension with increasing distance z . Instead, it becomes a function of z . Thus, assuming a small variation of the core radius, we can use Taylor series expansion [13] for β so that

$$\beta = \beta_0 + \left(\frac{\partial \beta}{\partial z} \right) z, \quad (4)$$

where the higher order terms are suppressed. In eq. (4) β_0 is the axial component of the propagation vector at the origin $z = 0$.

It can be shown that, using the transverse field components, the system of tapered guide will be represented by the equation [13]

$$\frac{\partial^2 \psi}{\partial \rho^2} + \frac{1}{\rho} \frac{\partial \psi}{\partial \rho} + \frac{1}{\rho^2} \frac{\partial^2 \psi}{\partial \phi^2} + \eta^2 \psi = 0, \quad (5)$$

where ψ is the field (i.e. E_z or H_z , as the case may be) and $\eta^2 = \omega^2 \mu \varepsilon - \beta^2$ with ε and μ ($\cong \mu_0$) as the permittivity and the permeability of the medium, respectively. It can also be shown that eq. (5) will have Bessel functions [42] as the solutions, and therefore, fields in the core/clad sections will be described by Bessel and the modified Bessel functions, and/or their linear combinations. The core region will have the expressions for E_z and H_z as

$$E_z(\rho < \rho_a) = C_1 J_\nu(u\rho) e^{j\nu\phi} e^{j(\omega t - \beta z)} \quad (6a)$$

and

$$H_z(\rho < \rho_a) = C_2 J_\nu(u\rho) e^{j\nu\phi} e^{j(\omega t - \beta z)}, \quad (6b)$$

respectively, whereas the clad section will have those as

$$E_z(\rho > \rho_a) = C_3 K_\nu(w\rho) e^{j\nu\phi} e^{j(\omega t - \beta z)}, \quad (7a)$$

$$H_z(\rho > \rho_a) = C_4 K_\nu(w\rho) e^{j\nu\phi} e^{j(\omega t - \beta z)}. \quad (7b)$$

In eqs. (6) and (7), C_1 , C_2 , C_3 and C_4 are arbitrary constants, the values of which can be determined by using the boundary conditions, and the parameters u and w are defined as

$$u^2 = \omega^2 \mu_0 \varepsilon_1 - \beta^2 = k_1^2 - \beta^2 \quad (8a)$$

and

$$w^2 = \beta^2 - \omega^2 \mu_0 \varepsilon_2 = \beta^2 - k_2^2, \quad (8b)$$

respectively. Implementing the longitudinal field components, one can explicitly obtain the transverse field components at an arbitrary radial point $\rho = \rho_a$ as

$$E_{\phi 1} = -\frac{j}{u^2} \left\{ \frac{j\nu\beta}{\rho_a} C_1 J_\nu(u\rho_a) - \mu_0 \omega C_2 u J'_\nu(u\rho_a) \right\} e^{j\nu\phi}, \quad (9a)$$

$$H_{\phi 1} = -\frac{j}{u^2} \left\{ \varepsilon_1 \omega C_1 u J'_\nu(u\rho_a) + \frac{j\nu\beta}{\rho_a} C_2 J_\nu(u\rho_a) \right\} e^{j\nu\phi}, \quad (9b)$$

$$E_{\phi 2} = \frac{j}{w^2} \left\{ \frac{j\nu\beta}{\rho_a} C_3 K_\nu(w\rho_a) - \mu_0 \omega C_4 w K'_\nu(w\rho_a) \right\} e^{j\nu\phi}, \quad (10a)$$

$$H_{\phi 2} = \frac{j}{w^2} \left\{ \varepsilon_2 \omega C_3 w K'_v(w \rho_a) + \frac{j v \beta}{\rho_a} C_4 K_v(u \rho_a) \right\} e^{j v t}. \quad (10b)$$

In eqs. (9) and (10), the suffixes 1 and 2, respectively, refer to the situations in the core and the clad sections, and the prime represents the differentiation with respect to the argument. Further, the propagation constant β is essentially governed by eq. (4).

2.2 Dispersion characteristics

According to the continuity conditions, the transverse field components must have a smooth match at the core/clad boundary, which will ultimately yield four equations, the solutions to which would exist only if the determinant formed by the coefficients is zero. This will finally provide the eigenvalue equation in β as [43]

$$(\aleph_v + \wp_v) \left(k_1^2 \aleph_v + k_2^2 \wp_v \right) - \left\{ \frac{v}{\rho_a} \left(\frac{1}{u^2} + \frac{1}{w^2} \right) \right\}^2 \left\{ \beta_0 + z \left(\frac{\partial \beta}{\partial z} \right) \right\}^2 = 0 \quad (11)$$

with

$$\aleph_v = \frac{J'_v(u \rho_a)}{u J_v(u \rho_a)},$$

$$\wp_v = \frac{K'_v(w \rho_a)}{w K_v(w \rho_a)}.$$

Under the approximation of very small RI difference, one would have $k_1^2 \approx k_2^2 \approx \beta^2$, and eq. (11) will acquire the form

$$\aleph_v + \wp_v = \pm \frac{v}{\rho_a} \left(\frac{1}{u^2} + \frac{1}{w^2} \right). \quad (12)$$

Using the recurrence relations for $J'_v(\cdot)$ and $K'_v(\cdot)$, there are two sets of equations for eq. (12) corresponding to the positive and the negative signs. The positive sign will yield

$$\frac{J_{v+1}(u \rho_a)}{u J_v(u \rho_a)} + \frac{K_{v+1}(w \rho_a)}{w K_v(w \rho_a)} = 0, \quad (13)$$

the solution to which will yield a set of EH modes. Corresponding to the negative sign, one would have

$$\frac{J_{v-1}(u \rho_a)}{u J_v(u \rho_a)} - \frac{K_{v-1}(w \rho_a)}{w K_v(w \rho_a)} = 0 \quad (14)$$

giving thereby a set of HE modes. Once again, using the recurrence relations, one can match all the tangential field components at the layer interface to obtain

$$\frac{uJ_{m-2}(u\rho_a)}{J_m(u\rho_a)} = -\frac{wK_{m-2}(w\rho_a)}{K_m(w\rho_a)}. \quad (15)$$

Eq. (15) represents the characteristic equation for the linearly polarized (LP) modes, where m is a new parameter defined as

$$m = \begin{cases} 1 & \text{for TE and TM modes} \\ \nu + 1 & \text{for EH modes} \\ \nu - 1 & \text{for HE modes} \end{cases} \quad (16)$$

However, under the limit $w \rightarrow 0$, one can obtain

$$\lim_{w \rightarrow 0} \frac{wK_{m-1}(w\rho_a)}{K_m(w\rho_a)} \rightarrow 0 \quad \text{for } m = 0, 1, 2, \dots \quad (17)$$

Under the circumstance, eq. (15) will assume the form

$$\frac{uJ_{m-2}(u\rho_a)}{J_m(u\rho_a)} = 0. \quad (18)$$

The solution to eq. (17) provides the knowledge of the dependence of the normalized propagation constant b on the normalized frequency parameter V [44]. The number of sustained modes in a guide (as a function of V) may be represented in terms of a normalized propagation constant

$$b = \frac{\rho_a^2 w^2}{V^2} = \frac{(\beta/k)^2 - n_2^2}{n_1^2 - n_2^2}. \quad (19)$$

In eq. (19), k is the free-space propagation constant. For a small index difference, eq. (19) reduces to the form

$$b \approx \frac{\left(\frac{\beta}{k}\right) - n_2}{n_1 - n_2}. \quad (20)$$

Under the limiting condition $w^2 \rightarrow 0$, the cutoff characteristic equation for the lowest mode ($\nu = 0$) of the fiber can be obtained as

$$J_0(u\rho_a) = 0. \quad (21)$$

If S_n represents the solutions to eq. (21) (with $n = 1, 2, 3$ etc. correspond to first, second, third etc. solutions), we would then have

$$u\rho_a = S_n. \quad (22)$$

One would finally obtain by implementing eqs. (4), (8a) and (21) that

$$z^2 \left(\frac{\partial \beta}{\partial z} \right)^2 + 2\beta_0 z \left(\frac{\partial \beta}{\partial z} \right) + \left\{ \beta_0^2 - k_1^2 + \left(\frac{S_n}{\rho_a} \right)^2 \right\} = 0. \quad (23)$$

Eq. (23) is essentially a quadratic equation in $\partial\beta/\partial z$, and it can be shown that, under the weak guidance approximation, the factor S_n in eq. (23) will have its value as 2.405 for the fundamental LP₁₁ mode [44]. Further, eq. (23) can be solved for $\partial\beta/\partial z$ numerically for different values of z . For a conventional fiber, the z -component of the propagation constant decreases with the decrease in fiber radius, and therefore, the propagation vector β should also decrease, making thereby a negative $\partial\beta/\partial z$. On the other hand, for increasing fiber radius (with z), $\partial\beta/\partial z$ must be positive. We thus consider the roots of eq. (23) so that those meet the physical situation. Fig. 2 depicts a plot of the variation of $\partial\beta/\partial z$ with z under the assumption of decreasing taper cross-section with the increase in z . We notice that the quantity $\partial\beta/\partial z$ increases rapidly with z near the origin; with the increase in the taper length, it shows a very small increase.

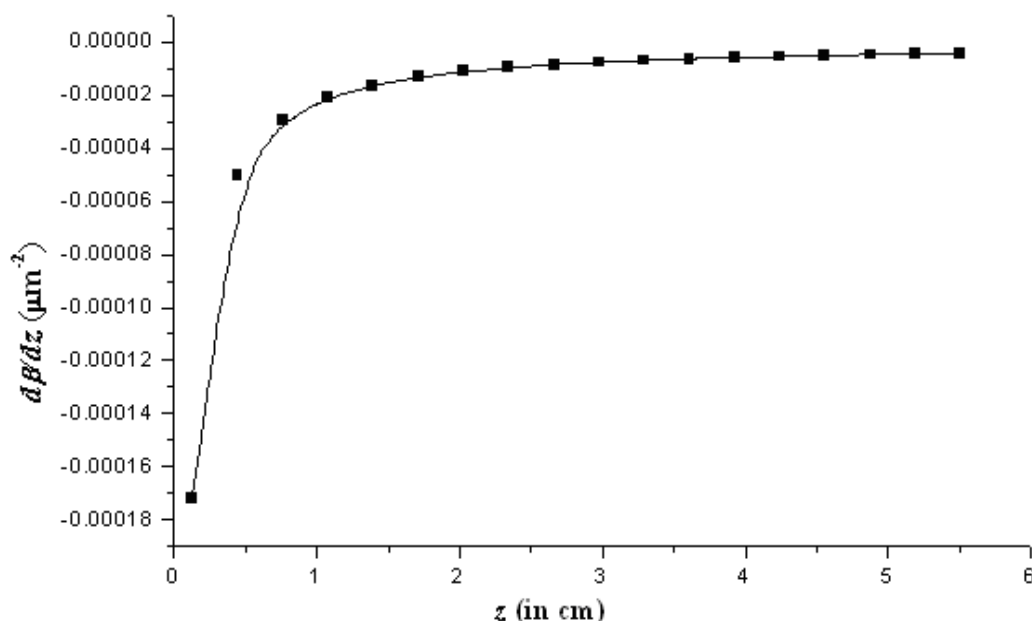


Fig. 2. Variation of $d\beta/dz$ with the longitudinal distance z .

We now make an attempt to analyze the dispersion relation for the TOF. We consider the fiber core as made of polystyrene material (with RI $n_1 = 1.6$) and the clad of methyl methacrylate (RI $n_2 = 1.48$). Step-index guides made of such materials are good candidates for low cost links. The operating wavelength is kept fixed at $1.55 \mu\text{m}$ because the attenuation of polystyrene materials is relatively low at this wavelength.

Fig. 3 illustrates the variation of the left hand side of eq. (11), as abbreviated as $f(u,w)$, with the dimensionless quantity $u\rho$. We observe the existence of the first intersection of the curve with the $f(u,w) = 0$ axis near $u\rho = 1$. Fig. 4 depicts the variation of the left hand side of eq. (17), as abbreviated as $f(u)$, with $u\rho$, which shows the cutoff value to be near $u\rho = 0.7$ - a value less than that obtained corresponding to fig. 3, as discussed above. As such, the results of figs. 3 and 4 remain consistent.

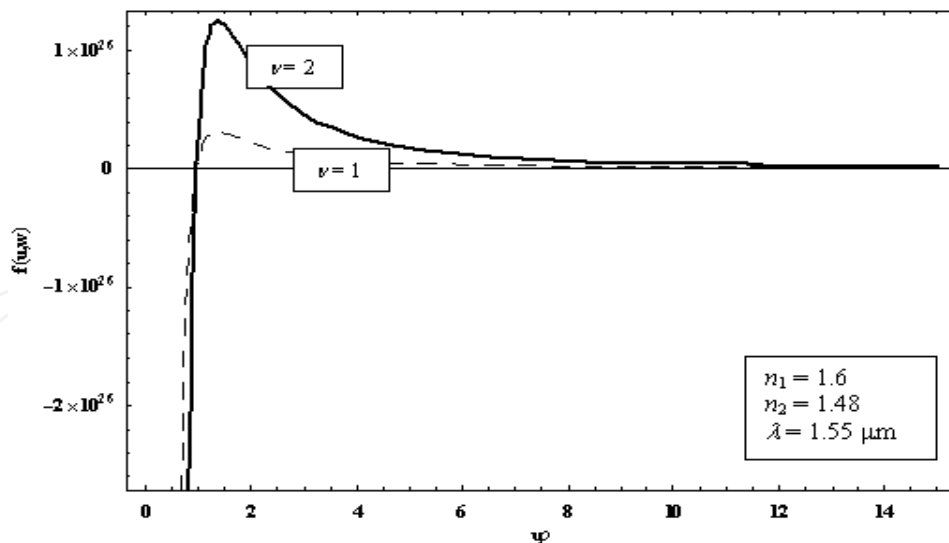


Fig. 3. Variation of the function $f(u, w)$ with $u\rho$.

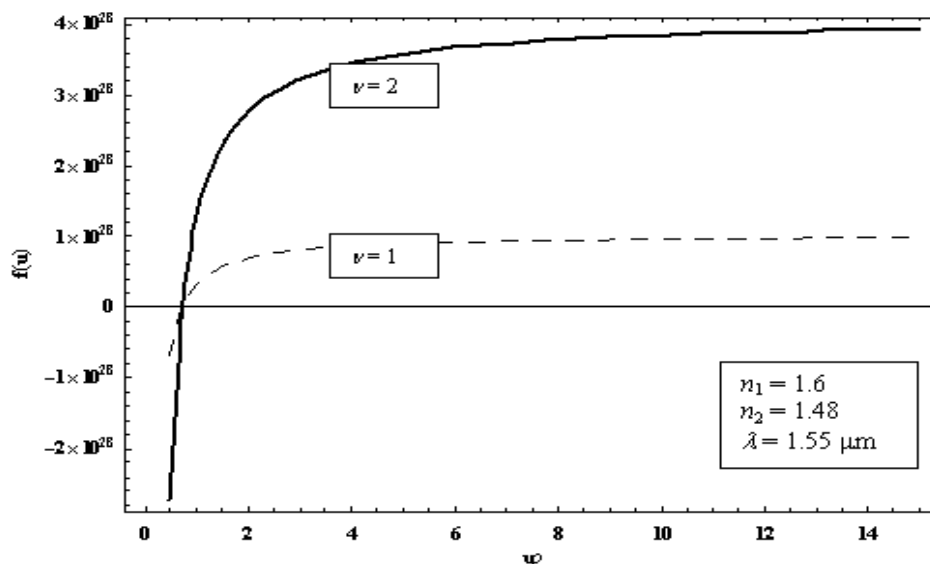


Fig. 4. Variation of the function $f(u)$ with the dimensionless quantity $u\rho$.

Fig. 5 represents the dispersion pattern of the TOF – the plot of b (in terms of β/k) against V – for a few low order modes. We observe each mode to exist only for values of $V < 2$. More explicitly, the cutoff values are crowded together in the region $V = 0.15 - 1.50$. The curves exhibit a tendency towards saturation near $V > 2.5$. Further, there exists another crowding for V -values exceeding 4.5. The modes are cutoff when $\beta/k = n_2$, and in this case, the modes exhibit cut off when $\beta/k = 1.48$. Only five modes (fig. 5) – HE_{11} , TE_{01} , TM_{01} , EH_{11} and HE_{12} – are found to exist in the tapered region of the TOF.

Fig. 6 depicts the variation of the normalized propagation constant b against the normalized frequency parameter V in terms of LP modes; five such modes are found to exist. We notice that, for a TOF with $0 < V < 0.5$, there will be only one guided mode, namely, LP_{01} mode. Similarly, for $0 < V < 1$, only LP_{01} and LP_{11} ; for $1 < V < 1.5$, only LP_{01} , LP_{21} and LP_{11} ; for $1.5 < V < 2$, only LP_{02} and LP_{03} guided modes exist. The number of modes decreases rapidly as V is reduced.

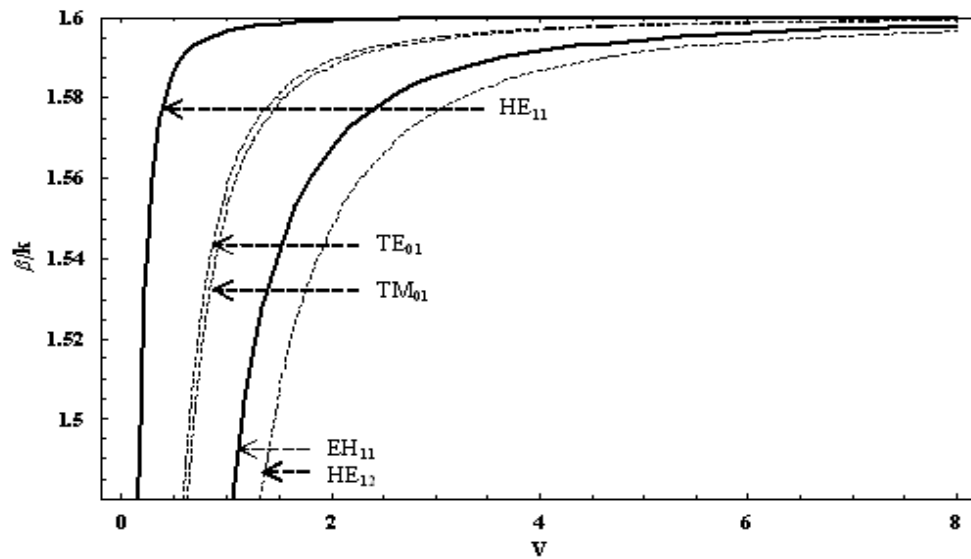


Fig. 5. Variation of β/k with the normalized frequency parameter V .

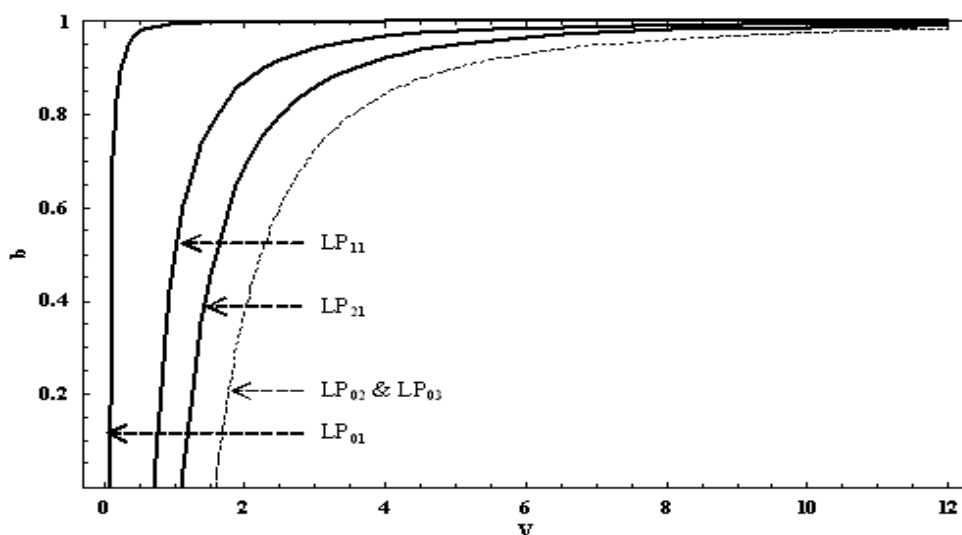


Fig. 6. Variation of the normalized propagation constant b with the normalized frequency parameter V .

A conventional circular core fiber becomes single-mode when $V < 2.405$ for which only the HE_{11} (or the LP_{01}) mode exists [44]. Comparing it with the present case of dielectric TOF, we observe that it becomes single-mode corresponding to the value of V approximately less than 0.7 (HE_{11} or LP_{01} mode exists in the fiber) – the feature attributed to the tapered geometrical nature of the guide. Thus, it can be inferred that the cutoff value is observed to greatly reduce in the case of dielectric TOFs.

2.3 Power propagation characteristics

The transmission of power [4,45] through the dielectric TOF remains important in the applications point of view. In the present subsection, we attempt to report the analysis of the

power confinement pattern in a dielectric TOF made of polystyrene core and clad with methyl methacrylate. Such plastic clad fibers (PCF) exhibit considerably greater attenuation than the conventional silica fibers. But, high numerical apertures and large acceptance angles of these PCFs essentially result in an easy launching of optical signals. The technique of split-step method, as discussed earlier, is implemented to deduce the formulations. The analysis becomes much rigorous through the implementation of Maxwell's field equations, and the results are ultimately obtained with much greater accuracy. The results presented in this subsection is aimed to provide the variation of the power confinement factor in the dielectric TOF core and the clad sections corresponding to some low order modes and different taper lengths.

As stated above, the continuity conditions require that the transverse EM field components should have a smooth match at the core/cladding interface. Based on this, and the above field eqs. (9) and (10), the amount of power [46] transmitted through the core and the clad sections can be explicitly given by the following expressions [47]:

$$\begin{aligned}
 P_{core} = & \frac{1}{2} \Re \int_0^{2\pi} \int_0^{\rho_a} C_1^2 \Xi \left[\left\{ \omega \varepsilon_1 u^2 \beta J_v'^2(u\rho) - \frac{\omega \varepsilon_1 u v^2 \beta}{\rho \rho_a} \Psi J_v(u\rho) J_v'(u\rho) \right. \right. \\
 & \left. \left. + \frac{v^4 \beta^3}{\rho^2 \rho_a} \Psi^2 J_v^2(u\rho) - \frac{u v^2 \beta^3}{\omega \mu_0 \rho_a \rho} \Psi J_v(u\rho) J_v'(u\rho) \right\} \right. \\
 & \left. - \left\{ \frac{u v^2 \beta^3}{\omega \mu_0 \rho_a \rho} \Psi J_v(u\rho) J_v'(u\rho) - \frac{\omega \varepsilon_1 v^2 \beta}{\rho^2} J_v^2(u\rho) - \frac{u^2 v^2 \beta^3}{\rho_a} \Psi^2 J_v^2(u\rho) \right. \right. \\
 & \left. \left. + \frac{\omega \varepsilon_1 u v^2 \beta}{\rho \rho_a} \Psi J_v(u\rho) J_v'(u\rho) \right\} \right] \rho d\rho d\phi
 \end{aligned} \tag{24}$$

and

$$\begin{aligned}
 P_{clad} = & \frac{1}{2} \Re \int_0^{2\pi} \int_{\rho_a}^{\infty} C_1^2 \Phi \left[\left\{ -\frac{\omega \varepsilon_2 w v^2 \beta}{\rho \rho_a} \Omega \frac{J_v(u\rho_a)}{K_v(w\rho_a)} K_v(w\rho) K_v'(w\rho) + \frac{v^4 \beta^3}{\rho^2 \rho_a} \Omega^2 K_v^2(w\rho) \right. \right. \\
 & \left. \left. + \frac{\omega \varepsilon_2 w^2 \beta J_v^2(u\rho_a) K_v'^2(w\rho)}{K_v^2(w\rho_a)} - \frac{v^2 w \beta^3}{\omega \mu_0 \rho_a \rho} \Omega \frac{J_v(u\rho_a)}{K_v(w\rho_a)} K_v(w\rho) K_v'(w\rho) \right\} \right. \\
 & \left. - \left\{ \frac{v^2 w \beta^3}{\omega \mu_0 \rho_a \rho} \Omega \frac{J_v(u\rho_a)}{K_v(w\rho_a)} K_v(w\rho) K_v'(w\rho) - \frac{\omega \varepsilon_2 v^2 \beta}{\rho^2} \frac{J_v^2(u\rho_a)}{K_v^2(w\rho_a)} K_v^2(w\rho) \right. \right. \\
 & \left. \left. - \frac{v^2 w^2 \beta^3}{\rho_a} \Omega^2 K_v'^2(w\rho) + \frac{\omega \varepsilon_2 v^2 w \beta}{\rho \rho_a} \Omega \frac{J_v(u\rho_a)}{K_v(w\rho_a)} K_v(w\rho) K_v'(w\rho) \right\} \right] \rho d\rho d\phi
 \end{aligned} \tag{25}$$

In eqs. (24) and (25), we used the symbols with their meanings as

$$\Xi = \frac{1}{(\omega^2 \mu_0 \varepsilon_1 - \beta^2)^2}, \quad \Psi = \frac{J_\nu(u\rho_a) \left(\frac{1}{u^2} + \frac{1}{w^2} \right)}{\frac{J'_\nu(u\rho_a)}{u} + \frac{J_\nu(u\rho_a) K'_\nu(w\rho_a)}{w K_\nu(w\rho_a)}},$$

$$\Omega = \frac{J_\nu^2(u\rho_a) \left(\frac{1}{u^2} + \frac{1}{w^2} \right)}{\frac{J'_\nu(u\rho_a) K_\nu(w\rho_a)}{u} + \frac{J_\nu(u\rho_a) K'_\nu(w\rho_a)}{w}}.$$

Further, in eqs. (24) and (25), the used constant C_1 is involved with the remaining constants C_2 , C_3 and C_4 as follows:

$$C_2 = \frac{j\nu\beta\Psi}{\omega\mu_0\rho_a} C_1, \quad (26a)$$

$$C_3 = \frac{J_\nu(u\rho_a)}{K_\nu(w\rho_a)} C_1, \quad (26b)$$

$$C_4 = \frac{j\nu\beta\Omega}{\omega\mu_0\rho_a} C_1. \quad (26c)$$

The constant C_1 in eqs. (26) can be determined by a normalization condition considering the input power.

Now, in the context of investigating the distribution of power in different TOF sections, figs. 7–9 illustrate the dependence of the power confinement factor along the tapered length. For the analysis, we keep the radius of the taper input ρ_i fixed to 50 μm , and the output taper cross-sectional size is varied. As stated earlier, the TOF core and the clad regions are, respectively, made of polystyrene (with RI $n_1 = 1.6$) and methyl methacrylate (RI $n_2 = 1.48$). The operating wavelength λ_0 is kept fixed at 1.55 μm . We present the plots of power for meridional ($\nu = 0$) and the lowest skew ($\nu = 1$) modes.

Figs. 7 and 8 illustrate the power confinement in the tapered core (against the taper length l) corresponding to the azimuthal mode indices $\nu = 0$ and 1, respectively. We take into account three different values of the output core radius, namely, 100 μm , 150 μm and 200 μm . We observe that the power confinement increases with the increase in output cross-sectional dimension, and also, the taper length. Corresponding to the meridional mode, the increase in power is fairly linear throughout the taper length; doubling of the output cross-section makes the power to increase by 20%. This increase in power is very much expected because fibers with larger dimensions transmit more amount of power.

Fig. 8 corresponds to the case of lowest skew mode with $\nu = 1$. We observe that, for smaller taper lengths, the power patterns show initially a sharp and fairly linear increase with the increase in taper length l . However, with the further increase in l , power increases, and ultimately reaches almost a saturation stage. Moreover, the nature of saturation becomes

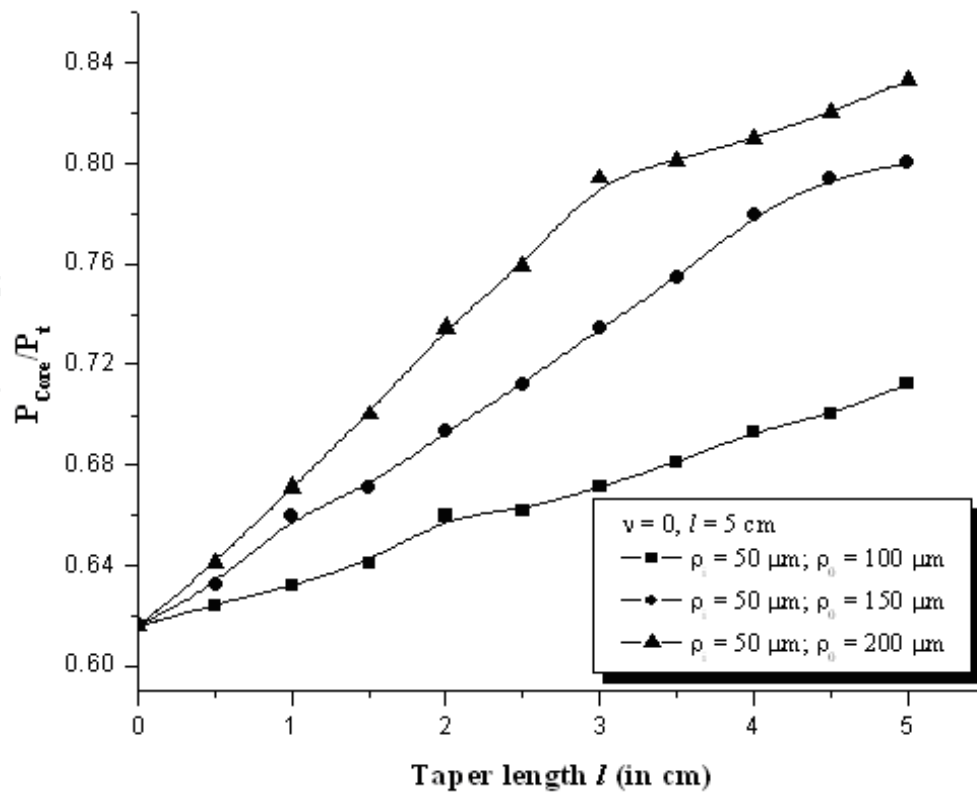


Fig. 7. Variation of core confinement factor corresponding to $\nu = 0$.

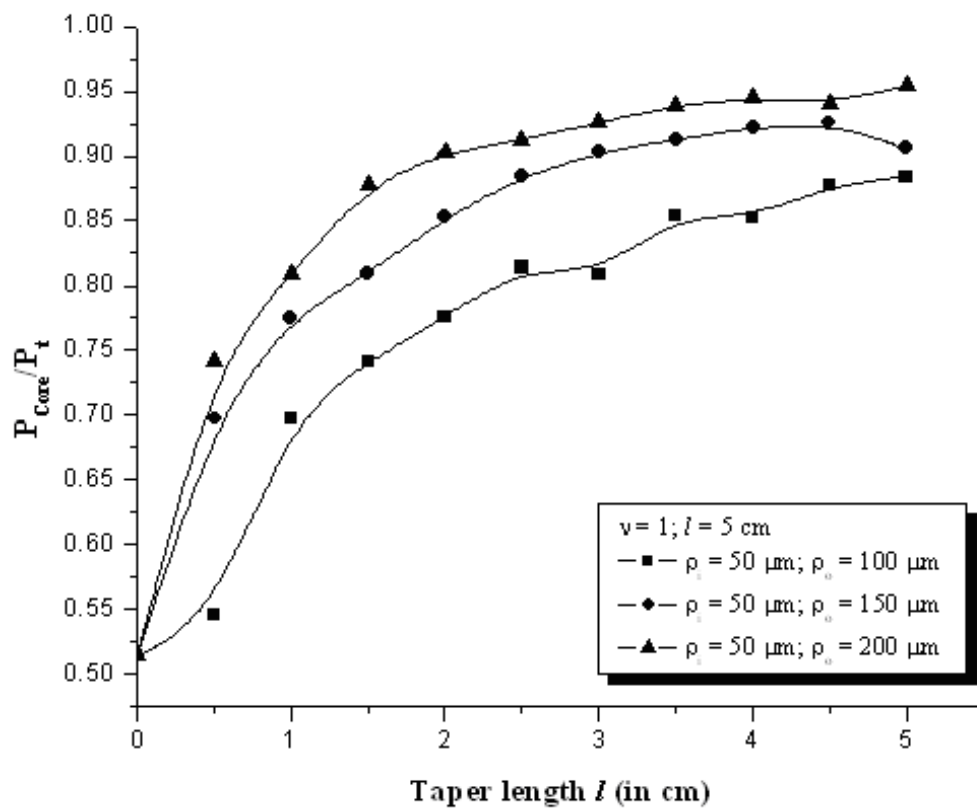


Fig. 8. Variation of core confinement factor corresponding to $\nu = 1$.

more pronounced corresponding to larger cross-sectional size. Fig. 8 also demonstrates that, for $\rho_i = 50 \mu\text{m}$ and $\rho_o = 200 \mu\text{m}$, and for larger taper lengths, more than 95% of power is confined in the TOF core, which determines that the skew modes transmit more amount of power as compared to the meridional modes. Further, skew modes transmit power better uniformly with increasing value of l - the rise in power is about 45% with the increase in output cross-section, and with the increase in taper length. As such, for skew modes, a fairly uniform distribution of power takes place among the sustained modes in this case - a desirable aspect for optical communications.

Fig. 9 depicts the power confinement with taper length corresponding to the meridional mode ($\nu = 0$). We observe that the confinement almost linearly decreases with increasing l , with a pronounced decrease for larger output cross-sections. Corresponding to the skew mode ($\nu = 1$; fig. 10), we observe that the confinement factor exhibits an initial sharp decrease in the clad section with increasing l , followed by relatively slower decrease with larger values of l . Further, the decrease in power is more corresponding to larger taper output cross-section (e.g. $200 \mu\text{m}$). Thus, the noticeable fact remains that, by increasing the output cross-sectional size, a markedly higher power is transmitted through the TOF core, and a pronounced decrease in power is observed in the TOF clad.

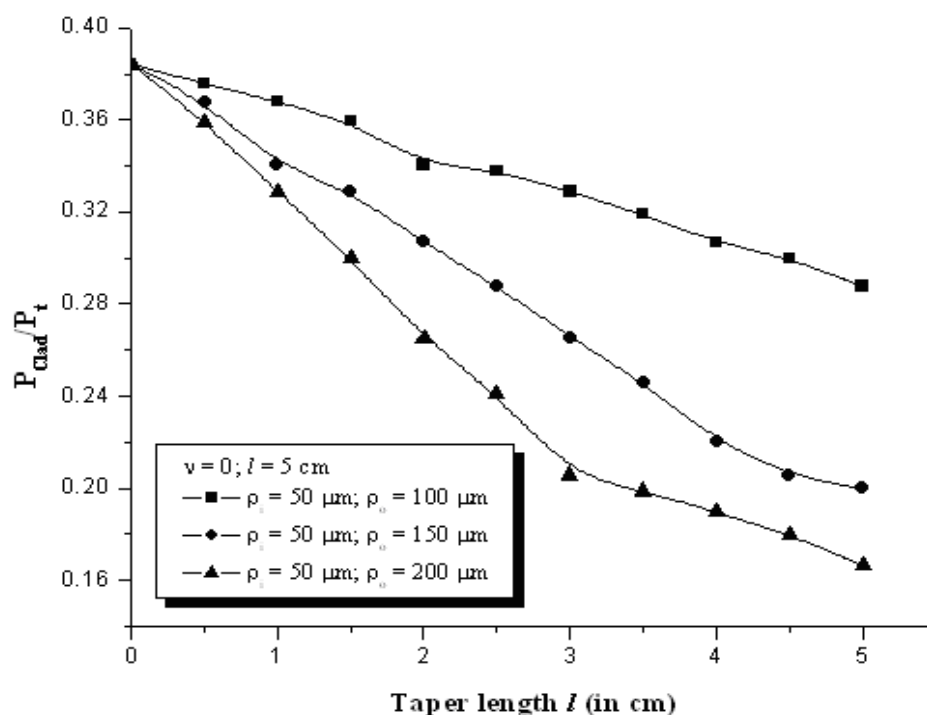


Fig. 9. Variation of clad confinement factor corresponding to $\nu = 0$.

Comparison of figs. 7-10 yields that a larger taper output dimension causes a fairly good uniformity in the distribution of power. However, it is noteworthy that the power distribution is also affected by the cross-sectional size at the taper input end. But, in our analysis, we fixed the taper input radius to $50 \mu\text{m}$. A physical interpretation of the uniformity in power distribution can be given in a way that, when the radii ρ_i and/or ρ_o of the tapered sections are small, it behaves like a few-mode component, making thereby the

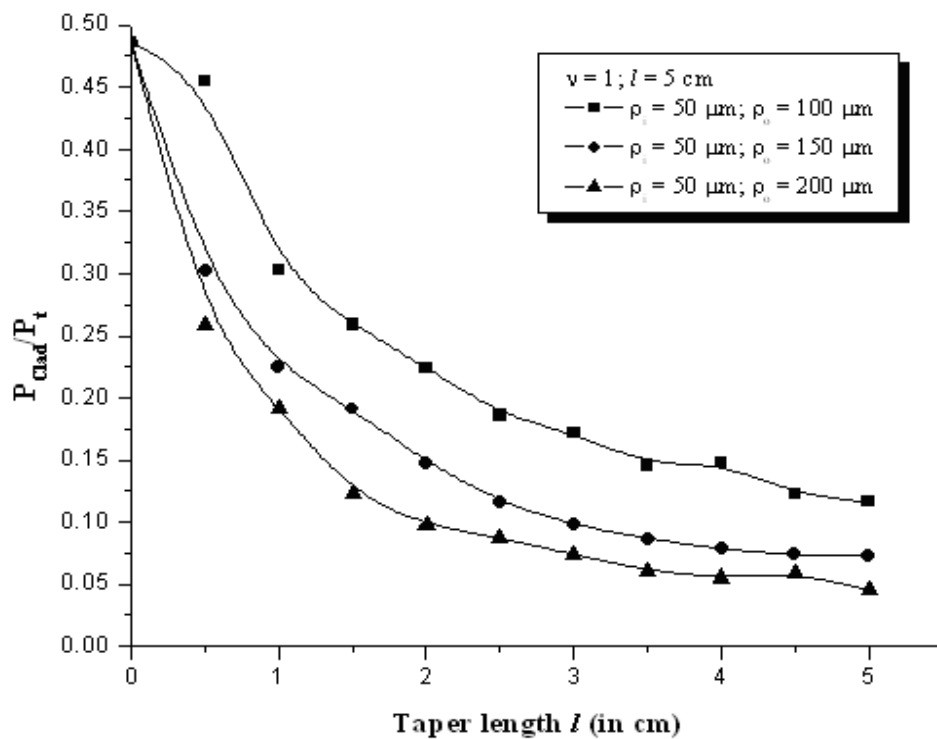


Fig. 10. Variation of clad confinement factor corresponding to $\nu = 1$.

power distribution patterns to bear some sort of *noisy* characteristics. The component starts behaving like a multimode structure corresponding to larger radii values – the feature more prominent in the case of skew modes.

3. Helical clad tapered dielectric optical fibers

Helical structures find enormous applications in low- and medium-power traveling wave tubes (TWTs) [35], the analyses of which generally include waveguides under slow-wave structures with conducting sheath and tape helices. The investigators have reported the implementation of this concept in the case of optical fibers [36]. As such, helical clad fibers, particularly with sheath helix patterns, fall among the category of new fiber types [48–54].

The analytical treatment of helical clad tapered fibers remains much complicated owing to the boundary conditions. The tapered structure may be handled by implementing the split-step method, similar to as discussed in the previous sections. An investigation of the dispersion characteristics of such tapered fibers with helical clads would be rather interesting as the helix pitch angle essentially plays a determining role to alter the dispersion behavior [50–54] of the guide.

In following subsections, we will deal with the preliminary ground work of helical clad dielectric TOFs, implementing a sheath helical pattern within the core-clad interface, because the purposely introduced helix pitch angle essentially brings in modifications in the dispersion profile. The use of Maxwell's equations can ultimately provide the dispersion relations for the structure, and the cutoff situations can be obtained under the chosen values of helix pitch.

3.1 Analytical approach

We consider a step-index linearly tapered helical clad optical fiber, as shown in fig. 11, the clad section of which is considered to be infinitely extended. A helical winding is introduced at the core/clad interface with the pitch angle as ψ . With the use of cylindrical polar coordinated (ρ, ϕ, z) , the wave propagation takes place along the direction of z , and the linear tapered function for structure is defined by eq. (2). The region $z < z_1$ in fig. 11 corresponds to the fiber pigtail, and that with $z > z_2$ to the expanded cylindrical section following the tapered section. The values of helix pitch angle $\psi = 0^\circ$ and $\psi = 90^\circ$ correspond to the two extreme situations - the former one indicates the winding to be perpendicular to the longitudinal direction whereas the latter one states those to be parallel to the z -axis. We assume that the core/clad sections are made of linear and isotropic non-magnetic materials, and therefore, $\mu_1 = \mu_2 \cong \mu_0$, the free-space permeability. Further, ε_1 and ε_2 are, respectively, the permittivity values of the core/clad sections.

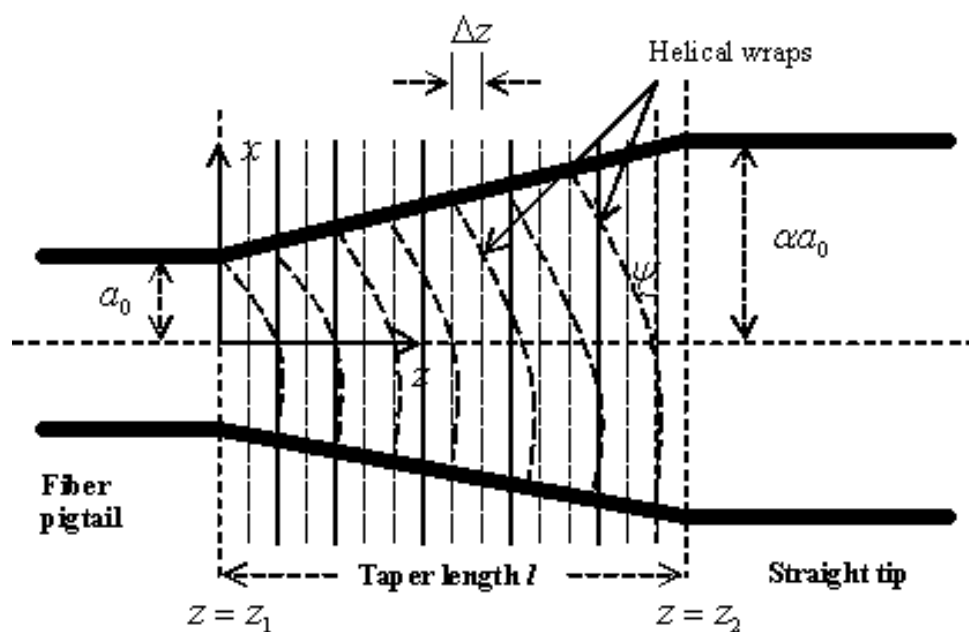


Fig. 11. Transverse view of TOF with helical wraps.

Considering the time t -harmonic and the axis z -harmonic EM fields, β becomes a function of the longitudinal distance z . Assuming a small variation of the core radius, the dependence of β may be expressed in the form of Taylor series expansion, as given in eq. (4). The longitudinal electric/magnetic fields in the core/clad sections will be described by Bessel and the modified Bessel functions, as shown in eqs. (6) and (7). Further, the transverse field components at an arbitrary radial point $\rho = \rho_n$ will be as given in eqs. (9) and (10).

3.2 Dispersion characteristics

The continuity conditions require that the transverse components of electric/magnetic fields at the core/clad boundary should get a smooth match. However, in the present case of helical clad fibers, the boundary conditions are essentially modified [35,55], which follows from the fact that the components of the electric field vanish in the direction of helix. Following that, a 4×4 matrix may be formed from the coefficients of the four unknowns in

four different equations, and the matrix should be vanishing in order to have a non-trivial solution to those four equations. In this way, the eigenvalue equation in β may be finally deduced as [56]

$$\begin{aligned} & u \frac{J_\nu(u\rho_a)}{J'_\nu(u\rho_a)} \left[\left(\sin\psi + \frac{\{\beta_0 + (\partial\beta / \partial z)z\} \nu}{u^2 \rho_a} \cos\psi \right)^2 \right] \\ & - w \frac{K_\nu(w\rho_a)}{K'_\nu(w\rho_a)} \left[\left(\sin\psi + \frac{\{\beta_0 + (\partial\beta / \partial z)z\} \nu}{w^2 \rho_a} \cos\psi \right)^2 \right] \\ & - \left[\frac{(k_1 n_1)^2}{u} \frac{J'_\nu(u\rho_a)}{J_\nu(u\rho_a)} - \frac{(k_2 n_2)^2}{w} \frac{K'_\nu(w\rho_a)}{K_\nu(w\rho_a)} \right] \cos^2 \psi = 0. \end{aligned} \quad (27)$$

Eq. (27) is the characteristic dispersion relation for helical clad tapered fibers. We may now consider two extreme values of the helix pitch angle ψ , namely $\psi = 0^\circ$ and $\psi = 90^\circ$, to be used to observe the effect of helix introduced at the core/clad interface. In this stream, when eq. (27) is solved for $\psi = 0^\circ$ (i.e. when the helical turns are perpendicular to the optical axis of the TOF), we finally obtain the characteristic dispersion relation as [56]

$$\begin{aligned} & u \frac{J_\nu(u\rho_a)}{J'_\nu(u\rho_a)} \left[\left(\frac{\{\beta_0 + (\partial\beta / \partial z)z\} \nu}{u^2 \rho_a} \right)^2 \right] - w \frac{K_\nu(w\rho_a)}{K'_\nu(w\rho_a)} \left[\left(\frac{\{\beta_0 + (\partial\beta / \partial z)z\} \nu}{w^2 \rho_a} \right)^2 \right] \\ & - \left[\frac{(k_1 n_1)^2}{u} \frac{J'_\nu(u\rho_a)}{J_\nu(u\rho_a)} - \frac{(k_2 n_2)^2}{w} \frac{K'_\nu(w\rho_a)}{K_\nu(w\rho_a)} \right] = f_1(u, w)(say) = 0. \end{aligned} \quad (28)$$

Corresponding to the case of helical turns being parallel to the optical axis (i.e. $\psi = 90^\circ$) of the TOF, eq. (27) provides [56]

$$u \frac{J_\nu(u\rho_a)}{J'_\nu(u\rho_a)} - w \frac{K_\nu(w\rho_a)}{K'_\nu(w\rho_a)} = f_2(u, w)(say) = 0. \quad (29)$$

Much changes in the shape of eqs. (28) and (29) essentially indicate the dominant effect of the helical clad in controlling the dispersion behavior of the guide. A deeper look at the dispersion relations under the helix pitch angles 0° and 90° (by solving eqs. (27) and (28), respectively) will numerically provide the values of the modal propagation constant β . In general, the dispersion equations may have multiple solutions for each value of azimuthal mode index ν . These solutions may be represented as $\beta_{\nu m}$; m being the order of the solution corresponding to a given value of ν . Each value of $\beta_{\nu m}$ corresponds to one possible mode. The limiting condition $w^2 \rightarrow 0$ determines the cutoff characteristics of the guide. Under the cutoff situations, corresponding to the helix pitch angles $\psi = 0^\circ$ and $\psi = 90^\circ$, we write the obtained equations in symbolic forms as $f_1(u) = 0$ and $f_2(u) = 0$, respectively.

In our computations, we consider the helical TOF as made of polystyrene core ($n_1 = 1.6$) and methyl methacrylate clad ($n_2 = 1.48$). Also, similar to the previous case, $\lambda_0 = 1.55 \mu\text{m}$ is the operating wavelength.

Fig. 12 illustrates the plot of $f_1(u, w)$ (based on eq. (28)) against the dimensionless quantity $u\rho$ corresponding to the perpendicular (to the axis) helical turns, i.e. $\psi = 0^\circ$. We chose two different illustrative values of the azimuthal mode index, viz. $\nu = 1$ and $\nu = 2$, and observe that the curves intersect the horizontal axis at around $u\rho = 0.65$. As such, there exist modes at this intersection point, and the exact values of the modal propagation constants may be evaluated.

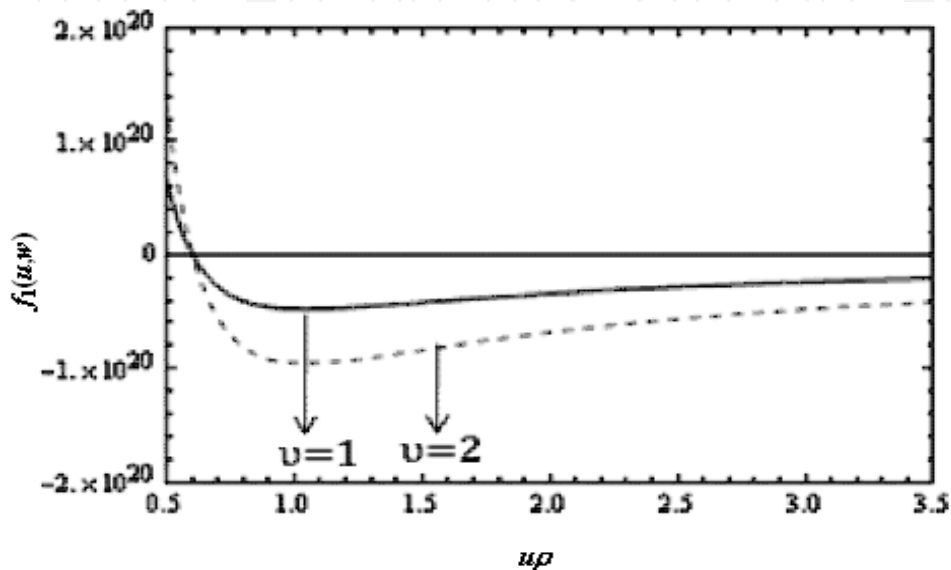


Fig. 12. Variation of the function $f_1(u, w)$ with $u\rho$ corresponding to $\psi = 0^\circ$.

Fig. 13 depicts the variation of $f_1(u)$ with the dimensionless quantity $u\rho$; $f_1(u)$ being the form of eq. (28), when solved under the limit $w^2 \rightarrow 0$ (not explicitly shown here). Thus, the cutoff variation of $f_1(u)$ corresponding to two values of the azimuthal index ν (namely, 1 and 2)

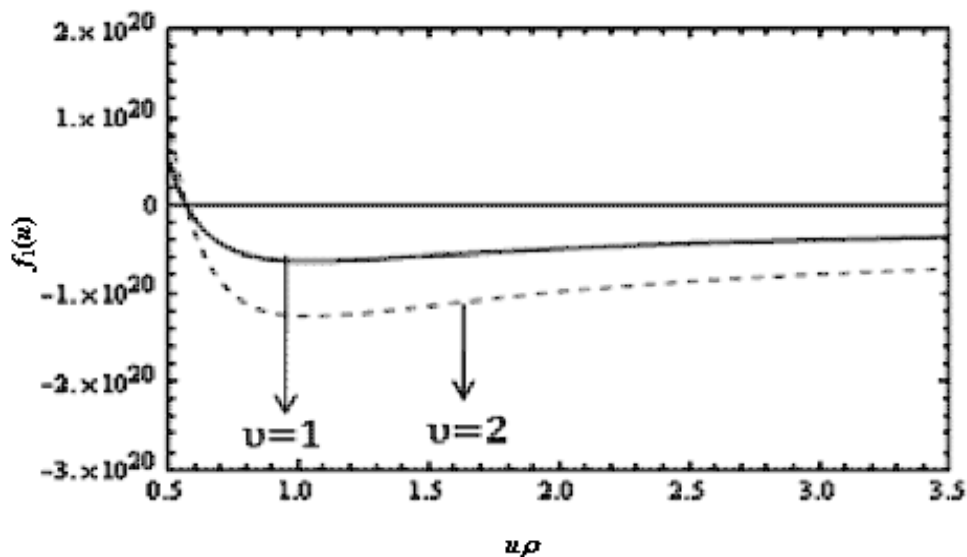


Fig. 13. Variation of the function $f_1(u)$ with $u\rho$ corresponding to $\psi = 0^\circ$.

shows the intersection with the horizontal axis at around $u\rho = 0.60$, which is less than the value of $u\rho (= 0.65)$, as observed in fig. 12. This shows the consistency of the results obtained in figs. 12 and 13. However, comparing the results with those reported earlier corresponding to the case of conventional dielectric TOFs without helical windings (Section 2; figs. 3 and 4), we observe that the existence of a helical wrap has the effect to increase the modal propagation constants.

Corresponding to the case of helical windings being parallel to the optical axis (i.e. $\psi = 90^\circ$), fig. 14 presents the plot of the left hand side $f_2(u,w)$ of eq. (29) against the dimensionless quantity $u\rho$ corresponding to the azimuthal mode index value as $\nu = 1$. We notice that the plot has the form of almost a straight line with the intersection at about $u\rho = 0.70$. Thus, as compared to the case of $\psi = 0^\circ$ (fig. 12), the $u\rho$ -crossing value becomes larger in this case, and therefore, the value of modal propagation constant decreases.

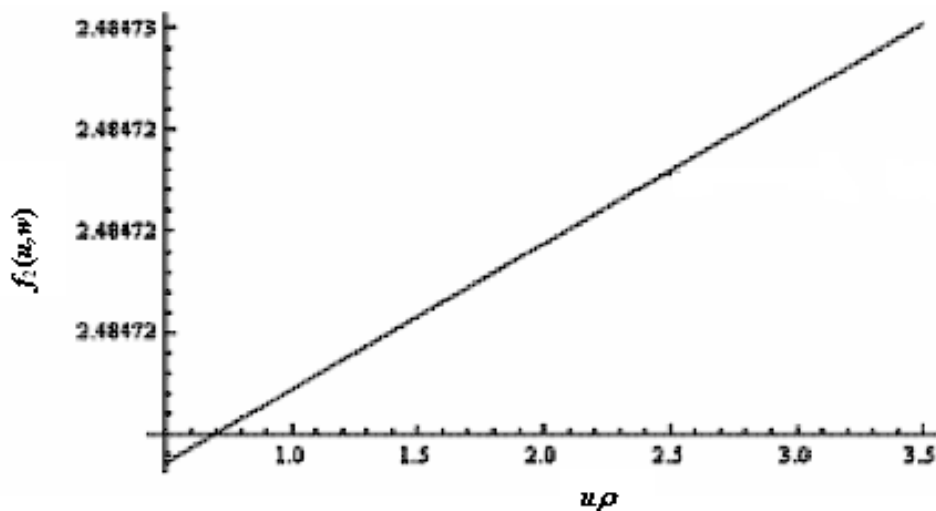


Fig. 14. Variation of the function $f_2(u,w)$ with $u\rho$ corresponding to $\psi = 90^\circ$ and $\nu = 1$.

Fig. 15 illustrates the cutoff characteristics when eq. (28) is solved under the limit $w^2 \rightarrow 0$. We notice the intersection in this case to be at around $u\rho = 0.60$ – a value less than that found

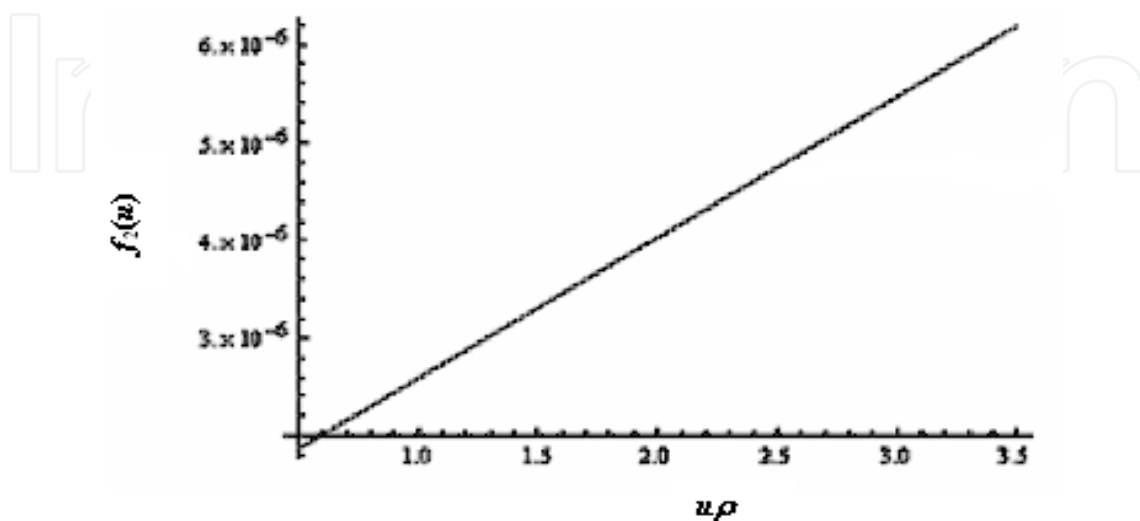


Fig. 15. Variation of the function $f_2(u)$ with $u\rho$ corresponding to the case of $\psi = 90^\circ$ and $\nu = 1$.

in fig. 12, indicating thereby the results of figs. 12 and 15 to be consistent. However, upon comparing the results with the case of dielectric TOFs without helical turns, we observe the general tendency that the helical clad TOFs increase the modal propagation constants. This essentially determines the controlling feature of the helical turns at the core/clad interface.

It can thus be inferred that, in helical clad TOFs, modes travel with higher propagation constants under the situation when the helical wraps are perpendicular to the optical axis of the guide than the case of parallel ones. However, compared with the situation of conventional dielectric TOFs, we observe that the existence of helix has the tendency to increase the modal propagation constants – the important role of the helix to control the propagation characteristics of dielectric TOFs.

4. Tapered fibers with liquid crystal clad

Liquid crystal optical fibers [37–39] possess several technological applications due to the fairly large polarization anisotropy [40] of liquid crystals. Owing to the large electro-optic coefficient of liquid crystals, the macroscopic optical properties of them can be manipulated by suitably applying external electrical fields.

In this section, we deal with the case of a three-layer liquid crystal tapered optical fiber (LCTOF) structure for which Maxwell's equations are implemented for a rigorous analysis. We consider the LCTOF having the outermost clad made of radially anisotropic liquid crystal material; the fiber core and the inner clad regions being made of isotropic dielectrics. It is to be pointed out here that the radial anisotropy of liquid crystals may be obtained by the capillary action after inserting the liquid crystal section into a capillary tube coated with N, N-dimethyl-N-octadecyl-3-aminopropyltrimethoxysilyl chloride.

A tapered structure of the fiber core is considered along the longitudinal direction because, as stated before, TOFs are of immense use in optical sensors and other in-line integrated optic applications. As such, an amalgamation of features in respect of fiber geometry and the material, i.e. a tapered core fiber with radially anisotropic outermost liquid crystal clad, would provide enhanced usefulness of the guide. With the advancement of the discussions, we concentrate on the dispersion profile corresponding to the low order TE and TM modes. Though the studies related to radially anisotropic LCTOFs have been reported before by Choudhury *et al.* [5], the present study provides a blend of liquid crystal material and tapered structure. We treat the LCTOF structure by implementing the split-step method, as discussed before.

4.1 Theory

Fig. 16(a) illustrates the cross-sectional view of LCTOF, which is made of homogeneous, isotropic and non-magnetic core and the inner clad. The outermost clad of the LCTOF is infinitely extended, and consists of radially anisotropic liquid crystal material. A comparison of the cases of radial and azimuthal anisotropies of the liquid crystal section makes the situation much clear; fig. 16(b) illustrates the case when the liquid crystal molecules assume azimuthal anisotropy; in figs. 16(a) and 16(b), the elongation of liquid crystal molecules is presented by dashed lines.

Fig. 17 represents the transverse view of the tapered nature of the fiber cross-section, where the core/inner clad sections have the RI values as n_1 and n_2 , respectively, with $n_1 > n_2$. Also,

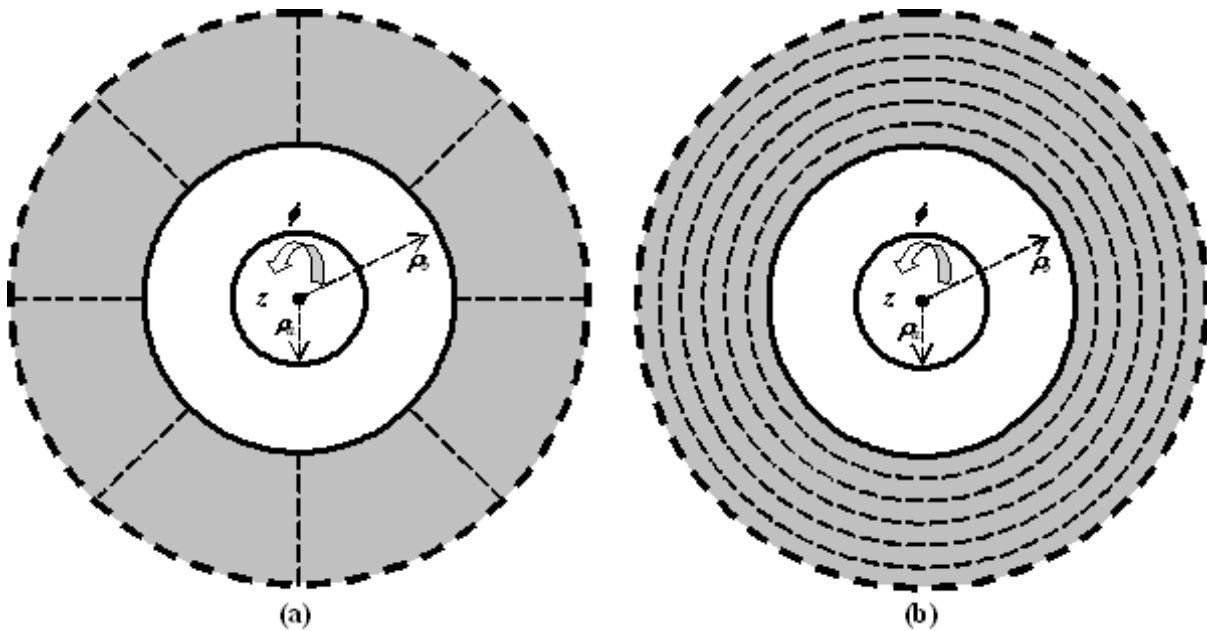


Fig. 16. LCTOF cross-section with nematic liquid crystal outermost clad (a) radial anisotropy, and (b) azimuthal anisotropy.

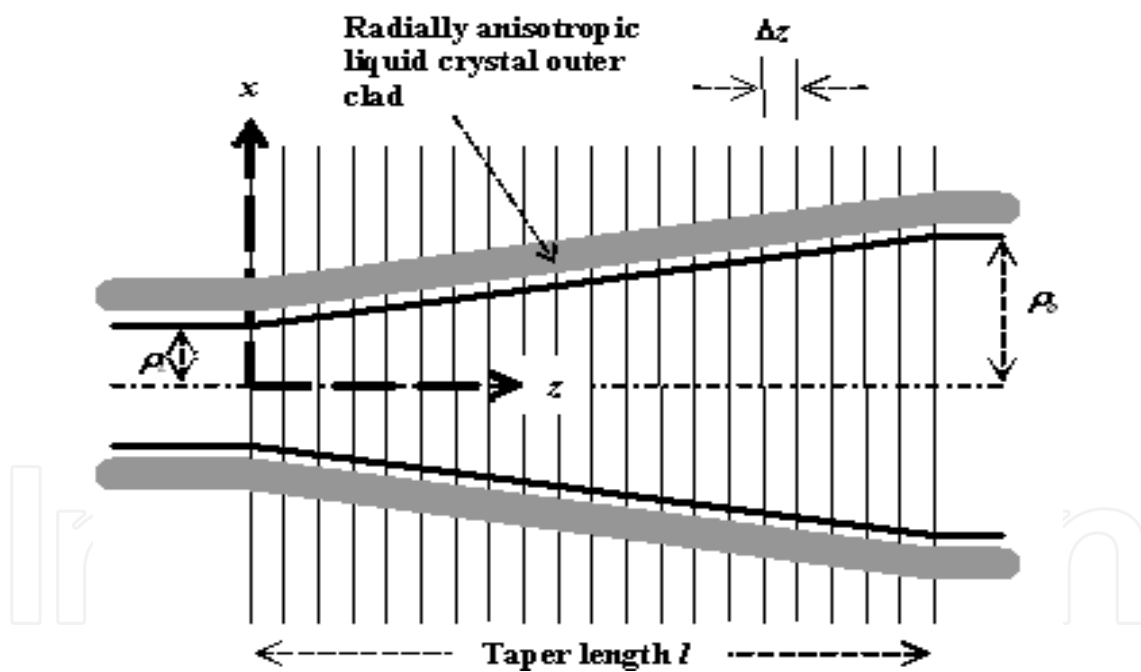


Fig. 17. Transverse view of the LCTOF of taper length l .

we consider the presence of radially anisotropic liquid crystal molecules in the infinitely extended outer clad with the ordinary and the extraordinary RI values as n_o and n_e , respectively. The linear taper nature of the fiber is defined by eq. (2).

The fiber geometry essentially needs the use of cylindrical polar coordinate system (ρ, ϕ, z) wherein the z -axis remains along the direction of wave propagation, and coincides with the principal axes of the outer clad. The extraordinary principal axis has a radial orientation, and therefore, the infinitely extended outer clad possesses the RI distribution given as

$n_\rho = n_e$ and $n_\phi = n_z$ with $n_e > n_1 > n_2 > n_o$,

as depicted figs. 18(a) and 18(b). Here n_ρ , n_ϕ and n_z are, respectively, the RI values along the ρ , ϕ and z -directions.

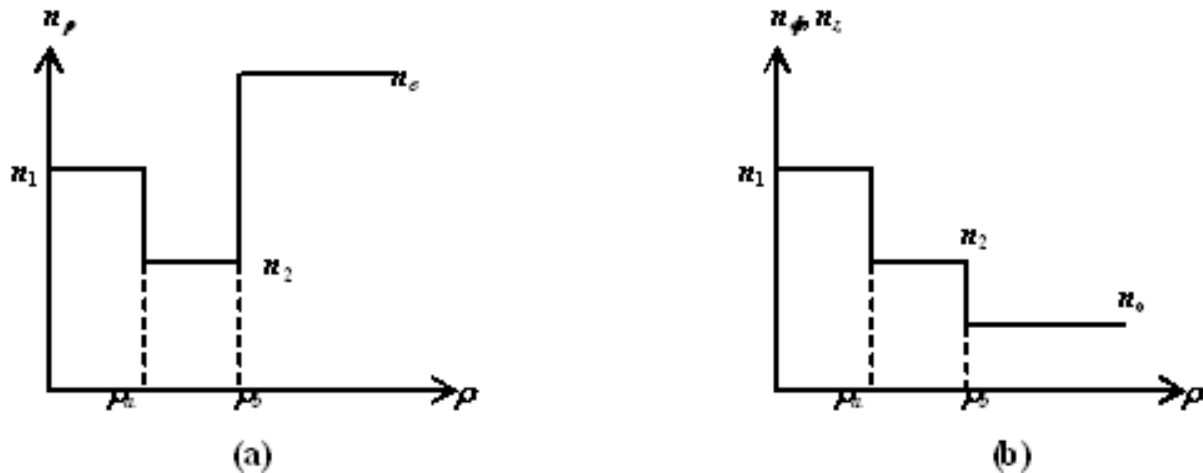


Fig. 18. The RI distribution pattern of the LCTOF.

Considering the time t -harmonic and the axis z -harmonic EM fields, coupled wave propagation equations for the transverse field components can be written as [5]

$$\left(\nabla_t^2 + k_0^2 n_\rho^2 - \beta^2 - \frac{1}{\rho^2} \right) e_\rho = -\frac{2}{\rho^2} \frac{\partial e_\phi}{\partial \phi} + \left(1 - \frac{n_\rho^2}{n_z^2} \right) \frac{\partial}{\partial \rho} \left\{ \frac{1}{\rho} \frac{\partial}{\partial \rho} (\rho e_\rho) \right\} + \left(1 - \frac{n_\phi^2}{n_z^2} \right) \frac{\partial}{\partial \rho} \left(\frac{1}{\rho} \frac{\partial e_\phi}{\partial \phi} \right), \quad (30a)$$

$$\left(\nabla_t^2 + k_0^2 n_\phi^2 - \beta^2 - \frac{1}{\rho^2} \right) e_\phi = \frac{2}{\rho^2} \frac{\partial e_\rho}{\partial \phi} + \frac{1}{\rho^2} \left\{ \left(1 - \frac{n_\rho^2}{n_z^2} \right) \frac{\partial}{\partial \rho} \left(\rho \frac{\partial e_\rho}{\partial \phi} \right) + \left(1 - \frac{n_\phi^2}{n_z^2} \right) \frac{\partial^2 e_\phi}{\partial \phi^2} \right\}. \quad (30b)$$

In eqs. (30), ∇_t^2 is the Laplacian operator in the cylindrical coordinate system, k_0 is the free-space propagation constant. Owing to the variation of the propagation constant β due to the varying cross-sectional dimension with distance z , β -values in eqs. (30) are governed by Taylor series expansion, as presented in eq. (4).

It is to be stated at this point that, in anisotropic guides, TE_{mn} , TM_{mn} and hybrid modes contain all the three electric field components E_ρ , E_ϕ and E_z . However, there are some special modes which do not contain all the three electric field components for which the index profiles in the zero electric field directions are irrelevant to the mode cutoff conditions. In our computations, we consider the lower order TE and TM modes, viz. TE_{01} and TM_{01} . For the TE_{01} mode, there is only one transverse electrical field component e_ϕ which is independent of the coordinate ϕ . Thus, corresponding to this mode, we have $e_\rho = 0$ and $\partial e_\phi / \partial \phi = 0$. On the other hand, for TM_{01} mode, there is only one non-zero component e_ρ , which is independent of the coordinate ϕ . Therefore, corresponding to the

TM₀₁ mode, we have $e_\phi = 0$ and $\partial e_\rho / \partial \phi = 0$. We will now treat the cases of TE and TM modes individually.

4.1.1 Transverse electric (TE) mode

As stated earlier, in the case of TE₀₁ mode we have $e_\rho = 0$ and $\partial e_\phi / \partial \phi = 0$. Using these in eq. (30b), the wave equation corresponding to TE modes in LCTOFs can be deduced as [5]

$$\frac{\partial^2 e_\phi}{\partial \rho^2} + \frac{1}{\rho} \frac{\partial e_\phi}{\partial \rho} + \left(k_0^2 n_\phi^2 - \beta^2 - \frac{1}{\rho^2} \right) e_\phi = 0. \quad (31)$$

In eq. (31), ρ and β are defined by eqs. (2) and (4), respectively. It can be shown that the solutions to eq. (31) will be in the form of combinations of Bessel and the modified Bessel functions. Using those solutions, harmony of the EM fields and Maxwell's field equations, the field components in the case of TE₀₁ mode may finally be obtained as follows [5]:

$$H_\rho = -\frac{\beta}{\omega \mu_0} e_\phi \exp\{j(\omega t - \beta z)\} \quad \text{with} \quad H_\rho = h_\rho \exp\{j(\omega t - \beta z)\}, \quad (32a)$$

$$H_z = \frac{j}{\omega \mu_0} \left(\frac{\partial e_\phi}{\partial \rho} + \frac{e_\phi}{\rho} \right) \exp\{j(\omega t - \beta z)\} \quad \text{with} \quad H_z = h_z \exp\{j(\omega t - \beta z)\}. \quad (32b)$$

In eqs. (32), μ_0 is the free-space permeability as the mediums are considered to be non-magnetic in nature. The use of eqs. (32) and the solutions to eq. (31) will ultimately provide the field components in the different fiber sections as follows [5]:

Core region:

$$H_\rho)_I = -A_{\phi 1} \frac{\beta}{\omega \mu_0} J_1(u\rho) \exp\{j(\omega t - \beta z)\}, \quad (33a)$$

$$H_z)_I = A_{\phi 1} \frac{j}{\omega \mu_0} \left\{ u J_1'(u\rho) + \frac{1}{\rho} J_1(u\rho) \right\} \exp\{j(\omega t - \beta z)\}. \quad (33b)$$

Inner clad region:

$$H_\rho)_II = -\frac{\beta}{\omega \mu_0} \left\{ A_{\phi 2} K_1(w\rho) + A_{\phi 3} I_1(w\rho) \right\} \exp\{j(\omega t - \beta z)\}, \quad (34a)$$

$$H_z)_II = \frac{j}{\omega \mu_0} \left[A_{\phi 2} \left\{ w K_1'(w\rho) + \frac{1}{\rho} K_1(w\rho) \right\} + A_{\phi 3} \left\{ w I_1'(w\rho) + \frac{1}{\rho} I_1(w\rho) \right\} \right] \exp\{j(\omega t - \beta z)\}. \quad (34b)$$

Outer clad region:

$$H_{\rho})_{III} = -A_{\phi 4} \frac{\beta}{\omega \mu_0} K_1(v\rho) \exp\{j(\omega t - \beta z)\}, \quad (35a)$$

$$H_z)_{III} = A_{\phi 4} \frac{j}{\omega \mu_0} \left\{ v K_1'(v\rho) + \frac{1}{\rho} K_1(v\rho) \right\} \exp\{j(\omega t - \beta z)\}. \quad (35b)$$

In eqs. (33), (34) and (35), $J(\bullet)$, $K(\bullet)$ and $I(\bullet)$ represent Bessel and the modified Bessel functions, and the prime stands for the differentiation with respect to the argument of the function. Also, $A_{\phi 1}$, $A_{\phi 2}$, $A_{\phi 3}$ and $A_{\phi 4}$ are the arbitrary constants to be determined by the boundary conditions.

4.1.2 Transverse magnetic (TM) mode

In the case of TM_{01} mode, since $e_{\phi} = 0$ and $\partial e_{\rho} / \partial \phi = 0$, eq. (30a) yields the wave equation for LCTOF as [5]

$$\frac{\partial^2 e_{\rho}}{\partial \rho^2} + \frac{1}{\rho} \frac{\partial e_{\rho}}{\partial \rho} + \left\{ (k_0^2 n_{\rho}^2 - \beta^2) \left(\frac{n_z}{n_{\rho}} \right)^2 - \frac{1}{\rho^2} \right\} e_{\rho} = 0. \quad (36)$$

In eq. (36) too, ρ is defined by eq. (2). Further, it can be shown that the non-zero field components for LCTOF in this case will assume the form [5]

$$E_z = -j \frac{n_e^2}{\beta n_0^2} \left(\frac{\partial e_{\rho}}{\partial \rho} + \frac{e_{\rho}}{\rho} \right) \exp\{j(\omega t - \beta z)\}, \quad (37a)$$

$$H_{\phi} = n_{\rho}^2 e_{\rho} \frac{\omega \epsilon_0}{\beta} \exp\{j(\omega t - \beta z)\}. \quad (37b)$$

Once again, in eqs. (37) too, ρ and β are considered to be according to as defined by eqs. (2) and (4), respectively. By using eqs. (37) and the solutions to eq. (36), the EM field components will be represented in this case as follows [5]:

Core region:

$$E_z)_{I} = -B_{\rho 1} \frac{j}{\beta \eta} \left\{ u J_1'(u\rho) + \frac{1}{\rho} J_1(u\rho) \right\} \exp\{j(\omega t - \beta z)\}, \quad (38a)$$

$$H_{\phi})_{I} = B_{\rho 1} \frac{\omega \epsilon_0}{\beta} n_{\rho}^2 J_1(u\rho) \exp\{j(\omega t - \beta z)\}. \quad (38b)$$

Inner clad region:

$$E_z)_{II} = -\frac{j}{\beta \eta} \left[B_{\rho 2} \left\{ w K_1'(w\rho) + \frac{1}{\rho} K_1(w\rho) \right\} \right]$$

$$+ B_{\rho 3} \left\{ w I_1'(w\rho) + \frac{1}{\rho} I_1(w\rho) \right\} \exp\{j(\omega t - \beta z)\}, \quad (39a)$$

$$H_{\phi})_{II} = \frac{\omega \varepsilon_0}{\beta} n_{\rho}^2 \{ B_{\rho 2} K_1(w\rho) + B_{\rho 3} I_1(w\rho) \} \exp\{j(\omega t - \beta z)\}. \quad (39b)$$

Outer clad region:

$$E_z)_{III} = -B_{\rho 4} \frac{j}{\beta \eta} \left\{ v' K_1'(v'\rho) + \frac{1}{\rho} K_1(v'\rho) \right\} \exp\{j(\omega t - \beta z)\}, \quad (40a)$$

$$H_{\phi})_{III} = B_{\rho 4} \frac{\omega \varepsilon_0}{\beta} n_{\rho}^2 K_1(v'\rho) \exp\{j(\omega t - \beta z)\}. \quad (40b)$$

In eqs. (38), (39) and (40), $B_{\rho 1}$, $B_{\rho 2}$, $B_{\rho 3}$ and $B_{\rho 4}$ are arbitrary constants to be defined by the boundary conditions, and the new quantities η and v' have the meanings as

$$\eta = (n_0 / n_e)^2 \quad (41)$$

and

$$v' = \frac{n_o}{n_e} \sqrt{n_e^2 k_0^2 - \beta^2}, \quad (42)$$

respectively.

4.2 Dispersion characteristics

4.2.1 Dispersion relation for TE mode

In order to obtain the dispersion relation, the continuity conditions of fields are to be imposed at the layer interface. As such, we consider the localized values of radial parameters (of LCTOF) to define the interface, e.g. we state $\rho = \rho_a$ as the core-inner clad interface and $\rho = \rho_b$ as the inner clad-outer clad interface; ρ_a and ρ_b , respectively, being the local parametric values of the LCTOF core and the inner clad radii. We now match the fields at the defined layer interfaces, which provide four equations altogether. Now, collecting the coefficients of the unknown arbitrary constants from those four equations, after a few lengthy steps, a 4×4 matrix can be deduced, as follows [57]:

$$\begin{pmatrix} \xi_{11} & -\xi_{12} & -\xi_{13} & 0 \\ 0 & \xi_{22} & \xi_{23} & -\xi_{24} \\ \xi_{31} & -\xi_{32} & -\xi_{33} & 0 \\ 0 & \xi_{42} & \xi_{43} & -\xi_{44} \end{pmatrix} = \Delta_{TE} \quad (\text{say}) = 0. \quad (43)$$

In eq. (43), various symbols have their meanings as follows:

$$\xi_{11} = (\beta / \omega \mu_0) J_v(u \rho_a), \quad \xi_{12} = (\beta / \omega \mu_0) K_v(w \rho_a),$$

$$\begin{aligned}
\xi_{13} &= (\beta / \omega\mu_0) I_v(w\rho_a), & \xi_{12} &= (\beta / \omega\mu_0) K_v(w\rho_b), \\
\xi_{23} &= (\beta / \omega\mu_0) I_v(w\rho_b), & \xi_{24} &= (\beta / \omega\mu_0) K_v(v\rho_b), \\
\xi_{31} &= (j / \omega\mu_0) \{uJ'_v(u\rho_a) + (1 / \rho_a) J_v(u\rho_a)\}, \\
\xi_{32} &= (j / \omega\mu_0) \{wK'_v(w\rho_a) + (1 / \rho_a) K_v(w\rho_a)\}, \\
\xi_{33} &= (j / \omega\mu_0) \{wI'_v(w\rho_a) + (1 / \rho_a) I_v(w\rho_a)\}, \\
\xi_{42} &= (j / \omega\mu_0) \{wK'_v(w\rho_b) + (1 / \rho_b) K_v(w\rho_b)\}, \\
\xi_{43} &= (j / \omega\mu_0) \{wI'_v(w\rho_b) + (1 / \rho_b) I_v(w\rho_b)\}, \\
\xi_{44} &= (j / \omega\mu_0) \{vK'_v(v\rho_b) + (1 / \rho_b) K_v(v\rho_b)\}.
\end{aligned}$$

Eq. (43) represents the dispersion relation for the LCTOF in the case when the TE modes are excited, and the solutions to this equation will provide different TE modes existing in the fiber under consideration. Further, it must be remembered that eq. (43), when solved under the limit $w^2 \rightarrow 0$, will provide the cutoff characteristics of the LCTOF.

4.2.2 Dispersion relation for TM mode

Following the procedure as discussed above for the case of TE modes, matching the field components at the localized radial parameters $\rho = \rho_a$ (core-inner clad interface) and $\rho = \rho_b$ (inner clad-outer clad interface), we finally obtain (after collecting the coefficients of the unknown constants) the dispersion relation (in the form of a 4×4 matrix) corresponding to the case of TM mode excitation of the LCTOF, as follows [57]:

$$\begin{pmatrix}
\zeta_{11} & -\zeta_{12} & -\zeta_{13} & 0 \\
0 & \zeta_{22} & \zeta_{23} & -\zeta_{24} \\
\zeta_{31} & -\zeta_{32} & -\zeta_{33} & 0 \\
0 & \zeta_{42} & \zeta_{43} & -\zeta_{44}
\end{pmatrix} = \Delta_{TM} \quad (\text{say}) = 0 \quad (44)$$

where the symbols have their meanings as given in the following:

$$\begin{aligned}
\zeta_{11} &= (j / \beta\eta^2) \{uJ'_v(u\rho_a) + (1 / \rho_a) J_v(u\rho_a)\}, \\
\zeta_{12} &= (j / \beta\eta^2) \{wK'_v(w\rho_a) + (1 / \rho_a) K_v(w\rho_a)\}, \\
\zeta_{13} &= (j / \beta\eta^2) \{wI'_v(w\rho_a) + (1 / \rho_a) I_v(w\rho_a)\}, \\
\zeta_{22} &= (j / \beta\eta^2) \{wK'_v(w\rho_b) + (1 / \rho_b) K_v(w\rho_b)\},
\end{aligned}$$

$$\zeta_{23} = (j / \beta \eta^2) \{ w I'_\nu(w \rho_b) + (1 / \rho_b) I_\nu(w \rho_b) \},$$

$$\zeta_{24} = (j / \beta \eta^2) \{ v K'_\nu(v \rho_b) + (1 / \rho_b) K_\nu(v \rho_b) \},$$

$$\zeta_{31} = (\omega \varepsilon_0 / \beta) n_\rho^2 J_\nu(u \rho_a), \quad \zeta_{32} = (\omega \varepsilon_0 / \beta) n_\rho^2 K_\nu(w \rho_a),$$

$$\zeta_{33} = (\omega \varepsilon_0 / \beta) n_\rho^2 I_\nu(w \rho_a), \quad \zeta_{42} = (\omega \varepsilon_0 / \beta) n_\rho^2 K_\nu(u \rho_a),$$

$$\zeta_{43} = (\omega \varepsilon_0 / \beta) n_\rho^2 I_\nu(w \rho_b), \quad \zeta_{44} = (\omega \varepsilon_0 / \beta) n_\rho^2 K_\nu(v \rho_b).$$

The solutions to eq. (44) will provide different TM modes existing in the LCTOF. Also, solving eq. (44) under the condition $w^2 \rightarrow 0$ will provide the LCTOF cutoff features.

4.2.3 Comparison of dispersion characteristics for TE and TM modes

Eqs. (43) and (44), corresponding to the TE and the TM mode excitations, provide the eigenvalue equations for the LCTOF. In the case of isotropic guides, viz. liquid crystal waveguides, TE and TM modes are difficult to separate owing to the reason that the direction independent RI values yield identical propagation constants and field cutoffs. However, the TE and the TM modes undergo different polarizations in such guides because of the direction dependent RIs, and therefore, these modes possess different values of propagation constants and field cutoffs.

We will now analyze these to determine the LCTOF characteristics in respect of their dispersion behavior and field cutoffs. The LCTOF in our consideration has three different sections with radially anisotropic liquid crystal outer clad. We take the RI values of the core and the inner clad as $n_1 = 1.5$ and $n_2 = 1.46$, respectively, and the outermost section has nematic liquid crystal as BDH mixture 14616 having the respective ordinary and the extraordinary RI values as $n_o = 1.457$ and $n_e = 1.5037$. We consider the excitation of low-order modes (with the azimuthal index ν as 1, 2 and 3), and the taper length l is taken to be 5 cm. Further, the localized values of the core and the inner clad radii are taken as $\rho_a = 60 \mu\text{m}$ and $\rho_b = 120 \mu\text{m}$, respectively, and the operating wavelength is kept as $1.55 \mu\text{m}$.

Fig. 19(a) presents the plots of the left hand side of eq. (43) corresponding to three different values of ν . The crossings of the curves with the horizontal axis represent the existence of modes with a particular value of the propagation constant β . We observe in fig. 19(a) that the zero crossings show a little increase with the increase in ν . We notice that the propagation constant β of the first mode corresponding to $\nu = 1$ is close to $5.935 \times 10^6 \text{ m}^{-1}$; β -values corresponding to the other existing modes can also be estimated from such intersections of the curves.

Eq. (43), when solved under the limit $w^2 \rightarrow 0$, gives the cutoff features under the TE mode excitation. Fig. 19(b) illustrates the cutoff situation of the TE modes. We observe that, when compared with the plots of fig. 19(a), the zero crossings of the curves indicate lesser cutoff β -values (for $\nu = 1$, the cutoff β -value is close to $5.918 \times 10^6 \text{ m}^{-1}$) than the β -values of the first existing mode. This essentially indicates that the results of figs. 19(a) and 19(b) are consistent.

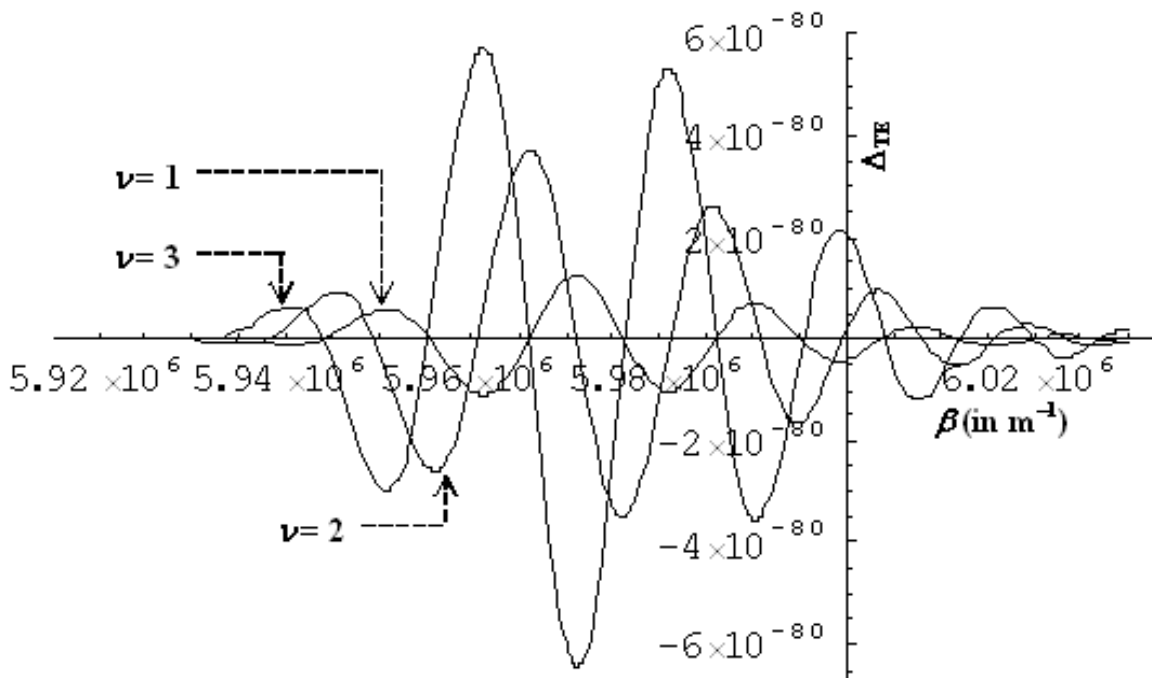


Fig. 19a. Plot of the dispersion relation for the TE modes.

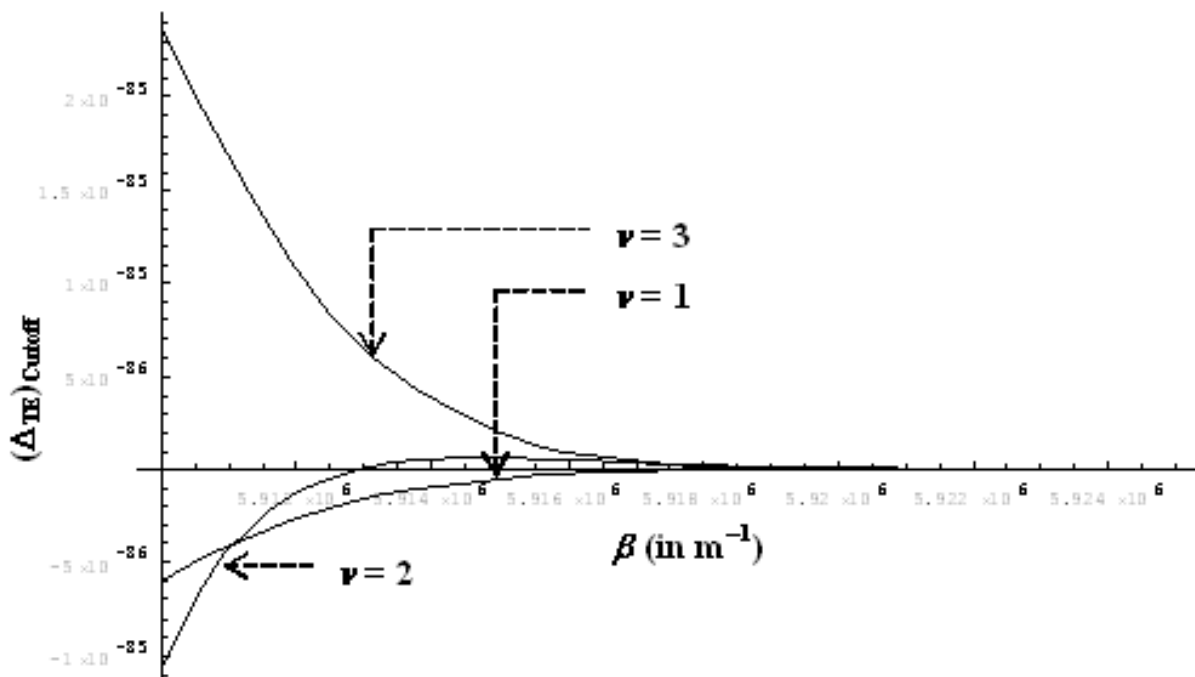


Fig. 19b. Plot of the cutoff characteristics for the TE modes.

Figs. 20 present the results corresponding to the TM modes for three different values of ν , namely 1, 2 and 3. Fig. 20(a) illustrates the plots of the left hand side of eq. (44), and fig. 20(b) corresponds to the cutoff plots when eq. (44) is solved under the limit $w^2 \rightarrow 0$. From fig. 20(a) we notice that the propagation constant for the first mode corresponding to $\nu = 1$ exists around $\beta = 6.076 \times 10^6 \text{ m}^{-1}$, which is smaller than the correspondingly observed zero crossing in the case of TE modes. Thus, as compared to the TE modes, the TM modes have the

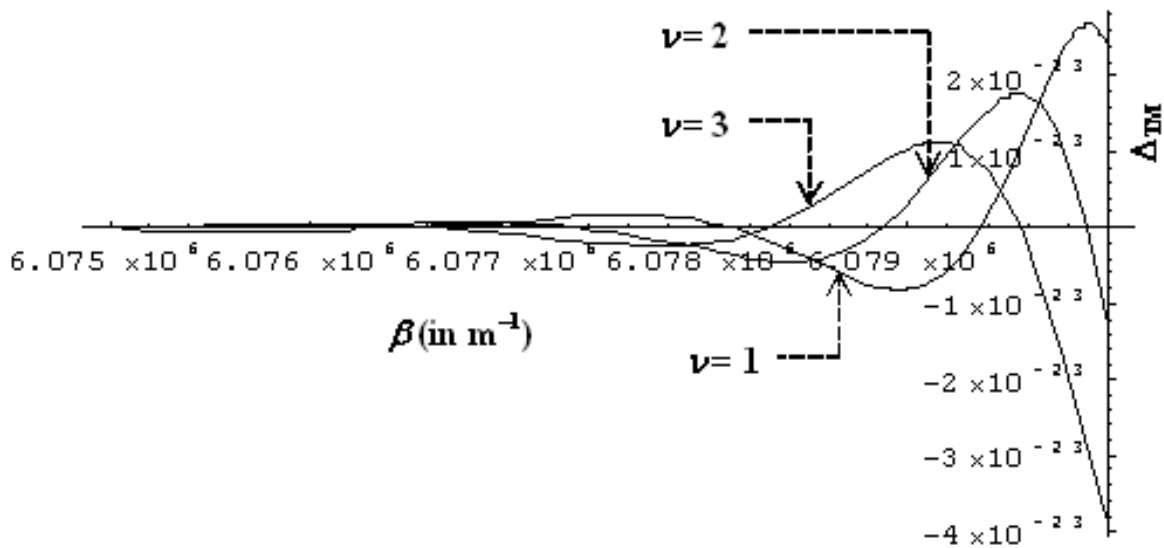


Fig. 20a. Plot of the dispersion relation for the TM modes.

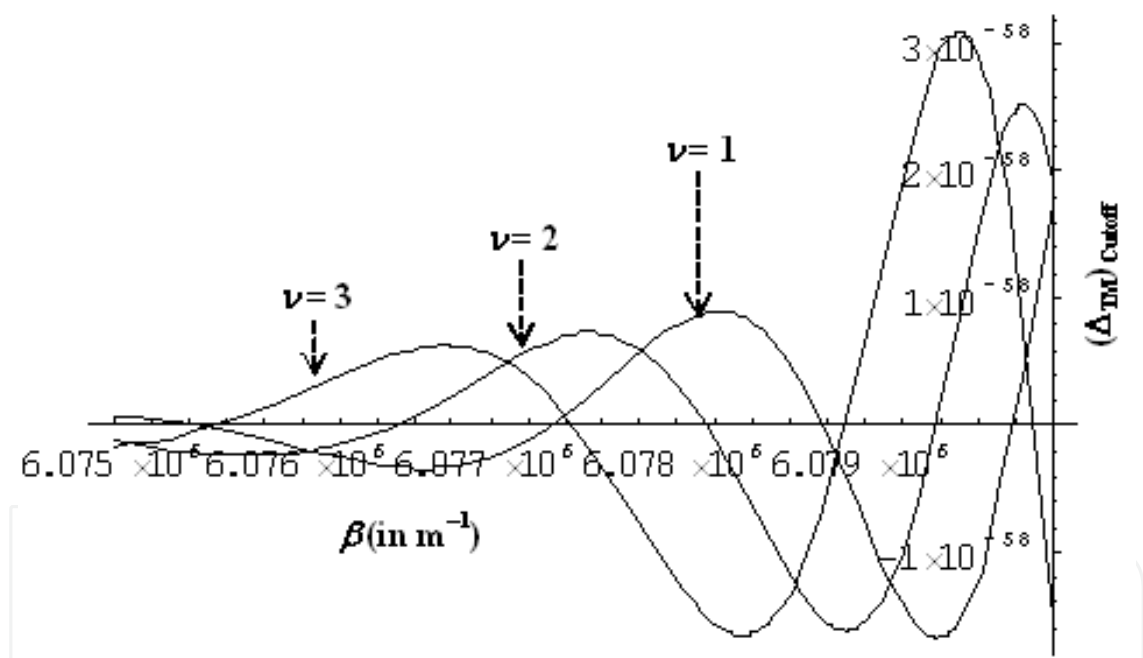


Fig. 20b. Plot of the cutoff characteristics for the TM modes.

tendency the lower the β -values. We also notice that the propagation constants increase with the increase in azimuthal index ν , which is similar to the situation observed in the case of TE modes. As observed from fig. 20(b) corresponding to the cutoff feature in the case of TM modes, the first zero crossings of the curves exist earlier than those seen in the corresponding plots in fig. 20(a), indicating thereby the consistency of the results presented in figs. 20(a) and 20(b). The analysis of the dispersion characteristics reveals the noticeable fact that the TE eigenmodes propagate in LCTOF with larger propagation constants as compared to the TM eigenmodes.

4.3 Features of power transport

As stated before, the individual useful properties of liquid crystal fibers and tapered fibers essentially motivate for the investigation of LCTOFs – the subject matter of the ongoing section. The applications of optical fibers are determined based on the power confinement characteristics. Thus, apart from the propagation behavior of the guide in terms of dispersion features and mode cutoffs, a glimpse of the power confinement factor remains equally important in order to emphasize the usefulness of the guide. As such, the discussion of the present subsection is pivoted to the analytical investigation of the power confinement in LCTOF structure. Using Maxwell's equations, a rigorous analysis is made of the confinement factors of the low order TE and TM modes sustained in the different LCTOF sections. In this context, variations in the core/clad dimensions are considered, and the illustrations are made of the power confinement factors against the length of the tapered section of the LCTOF.

4.3.1 Expressions of power for TE mode

In eqs. (33), (34) and (35), the values of arbitrary constants $A_{\phi 1}$, $A_{\phi 2}$, $A_{\phi 3}$ and $A_{\phi 4}$ can be evaluated by implementing the continuity conditions. Finally, after deducing the values of $A_{\phi 2}$, $A_{\phi 3}$ and $A_{\phi 4}$ in terms of $A_{\phi 1}$, the power [46] transmitted through the different sections of anisotropic LCTOF can be obtained as [58,59]

$$P_I = A_{\phi 1}^2 \frac{\pi}{\omega \mu_0} \left\{ u \int_0^{\rho_a} \rho J_1(u\rho) J_1'(u\rho) d\rho + \int_0^{\rho_a} (J_1(u\rho))^2 d\rho \right\}, \quad (45)$$

$$P_{II} = A_{\phi 1}^2 \frac{\pi}{\omega \mu_0} \left[C_1^2 \left\{ w \int_{\rho_a}^{\rho_b} \rho I_1(w\rho) I_1'(w\rho) d\rho + \int_{\rho_a}^{\rho_b} (I_1(w\rho))^2 d\rho \right\} \right. \\ \left. + C_2^2 \left\{ w \int_{\rho_a}^{\rho_b} \rho K_1(w\rho) K_1'(w\rho) d\rho + \int_{\rho_a}^{\rho_b} (K_1(w\rho))^2 d\rho \right\} + C_1 C_2 \left\{ 2 \int_{\rho_a}^{\rho_b} K_1(w\rho) I_1(w\rho) d\rho \right. \right. \\ \left. \left. + w \int_{\rho_a}^{\rho_b} \rho K_1(w\rho) I_1'(w\rho) d\rho + w \int_{\rho_a}^{\rho_b} \rho I_1(w\rho) K_1'(w\rho) d\rho \right\} \right], \quad (46)$$

$$P_{III} = A_{\phi 1}^2 \frac{\pi}{\omega \mu_0} \left(\frac{C_1 I_1(w\rho_b) + C_2 K_1(w\rho_b)}{K_1(v\rho_b)} \right)^2 \left[\int_{\rho_b}^{\infty} \{K_1(v\rho)\}^2 d\rho + v \int_{\rho_b}^{\infty} \rho K_1(v\rho) K_1'(v\rho) d\rho \right] \quad (47)$$

where

$$C_1 = \frac{w K_1'(w\rho_a) J_1(u\rho_a) + K_1(w\rho_a) \left\{ \frac{1}{\rho_a} (J_1(u\rho_a) - J_1(u\rho_a)) - u J_1'(u\rho_a) \right\}}{w K_1'(w\rho_a) I_1(w\rho_a) + K_1(w\rho_a) \left\{ \frac{1}{\rho_a} (I_1(w\rho_a) - K_1(w\rho_a)) - w I_1'(w\rho_a) \right\}}, \quad (48)$$

$$C_2 = \frac{I_1(u\rho_a) \left\{ wI_1'(w\rho_a) + \frac{1}{\rho_a} (K_1(w\rho_a) - I_1(w\rho_a)) \right\} - uJ_1'(u\rho_a)I_1(w\rho_a)}{K_1(w\rho_a) \left\{ wI_1'(w\rho_a) + \frac{1}{\rho_a} (K_1(w\rho_a) - I_1(w\rho_a)) \right\} - wK_1'(w\rho_a)I_1(w\rho_a)}. \quad (49)$$

Eqs. (45), (46) and (47), respectively, determine the power propagating through the fiber core, inner dielectric clad and the outer liquid crystal clad of the LCTOF under the situation when the TE modes are excited. In eqs. (45)–(49) ρ_a and ρ_b are the localized values of the LCTOF core and the inner clad radii, respectively; the outermost liquid crystal section is having an infinite extension. We used the split-step technique to analyze the problem, and ρ_a and ρ_b are the values of radii of a particular step. It is also to be remembered that the values of propagation constant β in all the equations are defined by eq. (4).

Further, in eqs. (45), (46) and (47), the constant $A_{\phi 1}$ can be determined by a normalization condition considering the input power. Now, if P_T is the total power transported by the TE₀₁ modes of LCTOF, i.e.

$$P_T = P_I + P_{II} + P_{III}, \quad (50)$$

then P_I/P_T , P_{II}/P_T and P_{III}/P_T will, respectively, determine the power confinement factor in the fiber core, inner clad and the outer clad of the LCTOF.

4.3.2 Expressions of power for TM mode

Following the above procedure implemented for TE modes, by the use of eqs. (38), (39) and (40) along with the continuity conditions, the expressions of power in the different sections of LCTOF under the TM mode excitation can finally be derived as [58,59]

$$p_I = B_{\rho 3}^2 \frac{\pi\omega\varepsilon_0 n_1^2}{\beta} \frac{I_1(w\rho_a)}{J_1(u\rho_a)} \left[1 + \frac{1 - \left(\frac{n_1}{n_2}\right)^2}{\left(\frac{n_1}{n_2}\right)^2 - 1} \right]^2 \left\{ \int_0^{\rho_a} \rho \{J_1(u\rho)\}^2 d\rho \right\}, \quad (51)$$

$$p_{II} = B_{\rho 3}^2 \frac{\pi\omega\varepsilon_0 n_2^2}{\beta} \left\{ \int_{\rho_a}^{\rho_b} \rho \frac{I_1(u\rho_a) \left\{ 1 - \left(\frac{n_1}{n_2}\right)^2 \right\}}{K_1(w\rho_a) \left\{ \left(\frac{n_1}{n_2}\right)^2 - 1 \right\}} K_1(w\rho) + I_1(w\rho) \right\}^2 d\rho \right\}, \quad (52)$$

$$p_{III} = B_{\rho 3}^2 \frac{\pi\omega\varepsilon_0 n_e^2}{\beta} \left[\frac{1}{K_1(v'\rho_b)} \left\{ I_1(w\rho_b) + \frac{K_1(w\rho_b)I_1(w\rho_a)}{K_1(w\rho_a)} \left(\frac{1 - \left(\frac{n_1}{n_2}\right)^2}{\left(\frac{n_1}{n_2}\right)^2 - 1} \right) \right\} \right]^2$$

$$\times \left\{ \int_{\rho_b}^{\infty} \rho \{K_1(v'\rho)\}^2 d\rho \right\}. \quad (53)$$

In eqs. (51), (52) and (53), the constant $B_{\rho\beta}$ can be determined by the normalization condition considering the input power. Now, if p_T is the total power transported by the TM modes of the LCTOF, i.e.

$$p_T = p_I + p_{II} + p_{III}, \quad (54)$$

then p_I/p_T , p_{II}/p_T and p_{III}/p_T will, respectively, determine the relative power distributions in the LCTOF core, inner clad and the outer clad regions. In eqs. (51), (52) and (53) too, the parameters ρ_a , ρ_b and β will assume the forms as described above in the case of TE modes.

4.3.3 Analysis of power transmission by TE and TM modes

We now analyze the LCTOF characteristics in respect of the power confinement factors (or the relative power distributions) corresponding to the cases of TE and TM modes. In our computations, we consider the core/inner clad RI values as $n_1 = 1.462$ and $n_2 = 1.458$, respectively. Further, as stated before, the infinitely extended outermost section is taken to be nematic liquid crystal BDH mixture 14616 having the respective ordinary and extraordinary RI values as $n_o = 1.457$ and $n_e = 1.5037$. For simplicity, we considered the modes with the azimuthal index value $\nu = 1$. The taper length l is taken to be 5 cm and the operating wavelength as $1.55 \mu\text{m}$.

Figs. 21a, 21b and 21c illustrate the logarithmic plots of the power confinement patterns in the core, the inner clad and the outer clad, respectively, of the LCTOF under the case of TE mode excitation, and the azimuthal mode index $\nu = 1$. While obtaining this, the input end core radius of the LCTOF tapered region is taken to be fixed (as $60 \mu\text{m}$) whereas the output end core radius is varied (to be as $80 \mu\text{m}$, $100 \mu\text{m}$, $120 \mu\text{m}$ and $140 \mu\text{m}$). We observe in these figures that the confinement factor increases with the increase in taper length along the direction of propagation; the lowest value of confinement corresponds to the situation when the outer core radius remains minimum (i.e. $80 \mu\text{m}$). This becomes explicit because lesser amount of power is transported by the guides of lower dimensions. Apart from this, a gradual increase in power confinement remains due to a steady increase in the LCTOF dimension as the wave propagates across the tapered section. We also notice that the confinement reaches a kind of saturation in the region near the output end of the tapered section.

Further analysis of figs. 21 reveals that, apart from the trend of increase in confinement factor, a very small amount of power is confined within the tapered core section (fig. 21a), and this feature sustains with all the chosen dimensions of LCTOF. Corresponding to the similar values of fiber dimensions and other operating conditions, the confinement is increased in the inner clad (fig. 21b) along with the trend of its variation remaining almost same, as that noticed in fig. 21a. The confinement shows a pronounced enhancement in the outer clad (fig. 21c), and remains maximum in this region. It is also seen that the increase in confinement in the outermost liquid crystal section simultaneously causes to decrease the same in the LCTOF core or the inner clad, and this may be viewed in a way as if the power

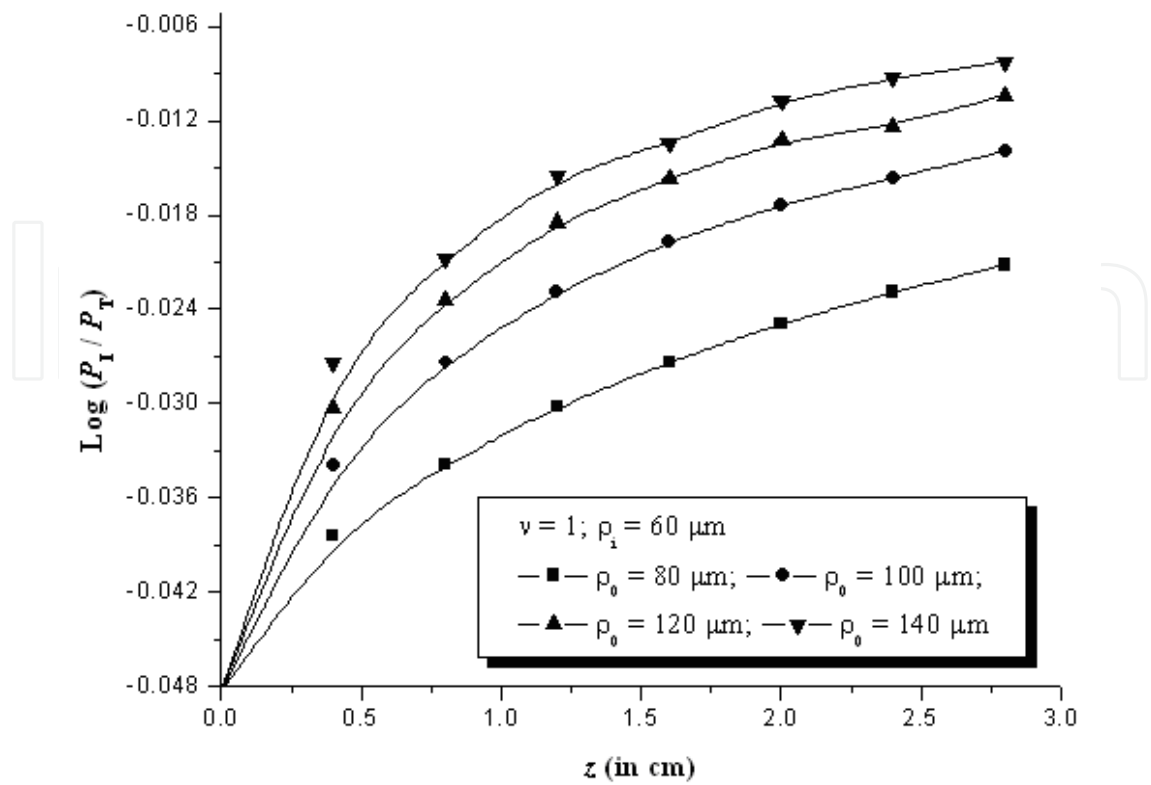


Fig. 21a. TE mode power confinement in LCTOF core.

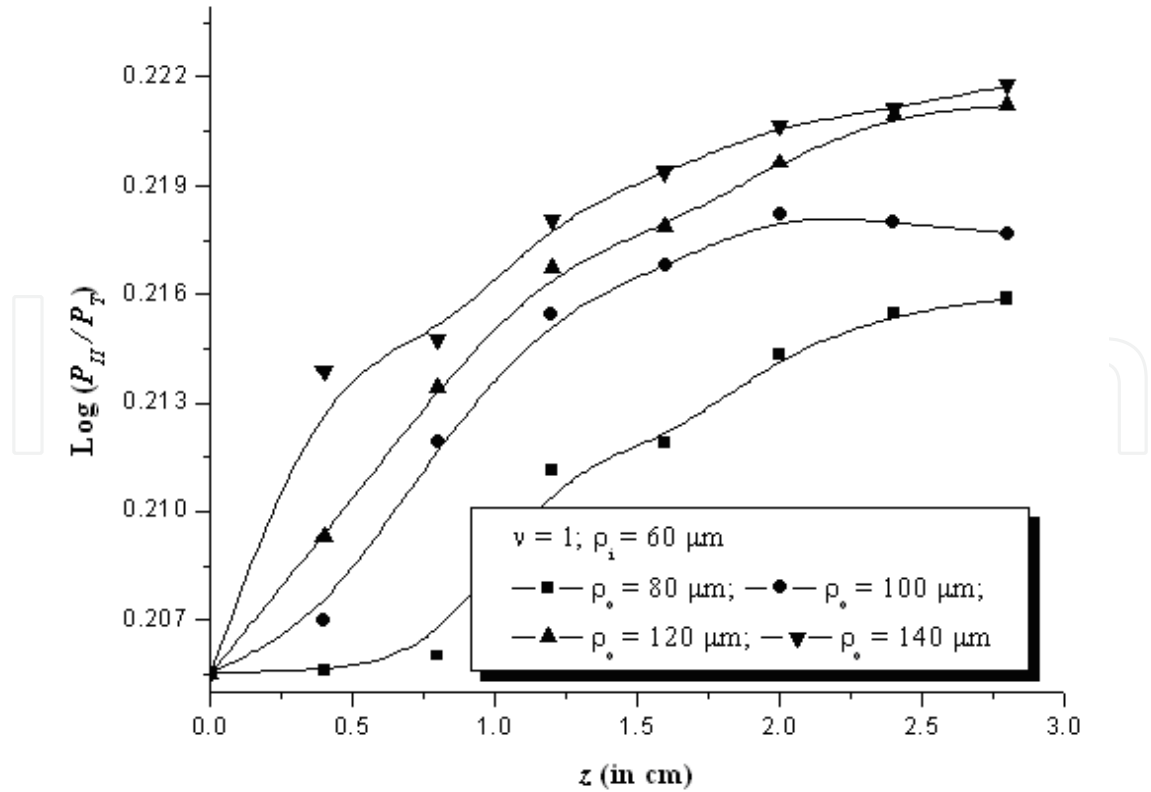


Fig. 21b. TE mode power confinement in the inner clad of LCTOF.

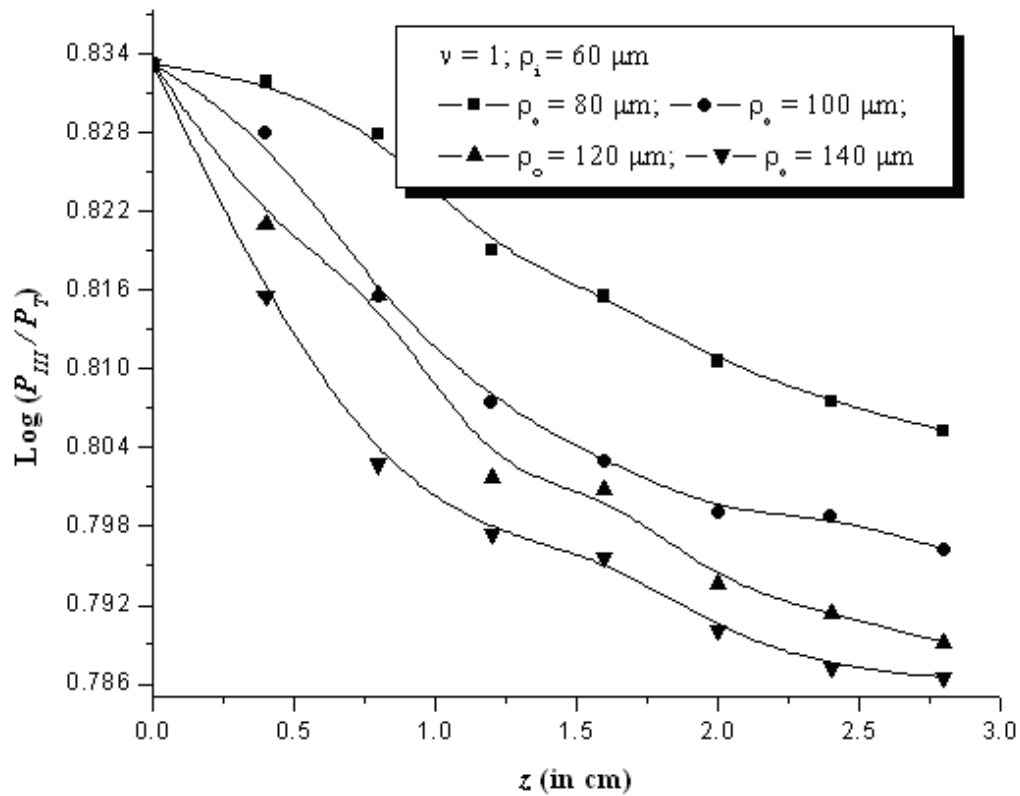


Fig. 21c. TE mode power confinement in the outermost clad of LCTOF.

is *leaking off* the fiber core, and propagating through the clad. This feature is essentially attributed to the presence of liquid crystal in the outermost clad region, and is of much use in sensing applications.

Figs. 22 correspond to the logarithmic variations of the power confinement for TE modes with $\nu = 1$ when the output end radius of the tapered core is fixed as $100 \mu\text{m}$, and the input end radius is varied. We observe from the figures that the power confinement remains maximum corresponding to the minimum value of the input core radius (i.e. $10 \mu\text{m}$). With the increase in LCTOF core input end radius, the confinement becomes uniform without exhibiting much change along the taper length, and this is very much obvious as the taper section undergoes maximum variation in respect of its dimensional structure along its length with minimum value of radius of the input end.

Fig. 22a shows that the power confinement remains almost uniform when the core radius at the input end is $70 \mu\text{m}$, and it presents maximum variation corresponding to the situation when the input end core radius is $10 \mu\text{m}$. On comparing figs. 22a, 22b and 22c we observe that the maximum amount of power confinement is attained in fig. 22c. This is just a replica of the situation that we observe in figs. 21c – the maximum amount of power is confined in the outermost section of the LCTOF. This feature of LCTOF is expected to find prominent usefulness in optical sensing, particularly the situations when the evanescent field sensing remains the best option. Apart from sensing, such a characteristic of LCTOF would also be useful in field coupling devices, wherein a relatively high amount of power is required to be present in the outermost section of the fiber.

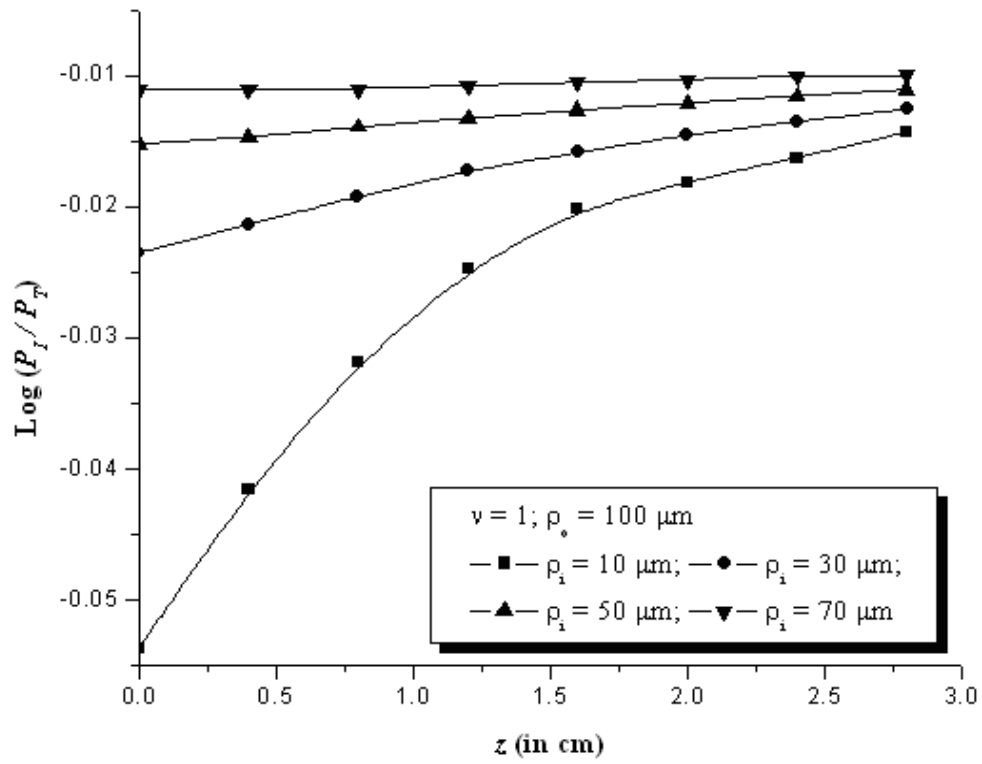


Fig. 22a. TE mode power confinement in LCTOF core.

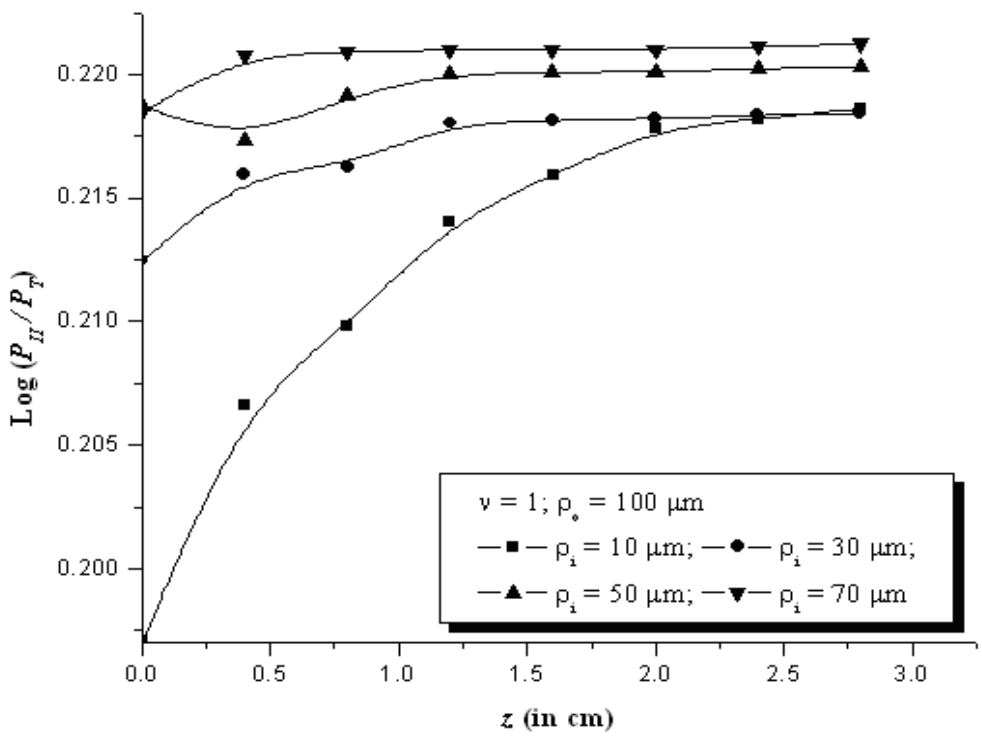


Fig. 22b. TE mode power confinement in the inner clad of LCTOF.

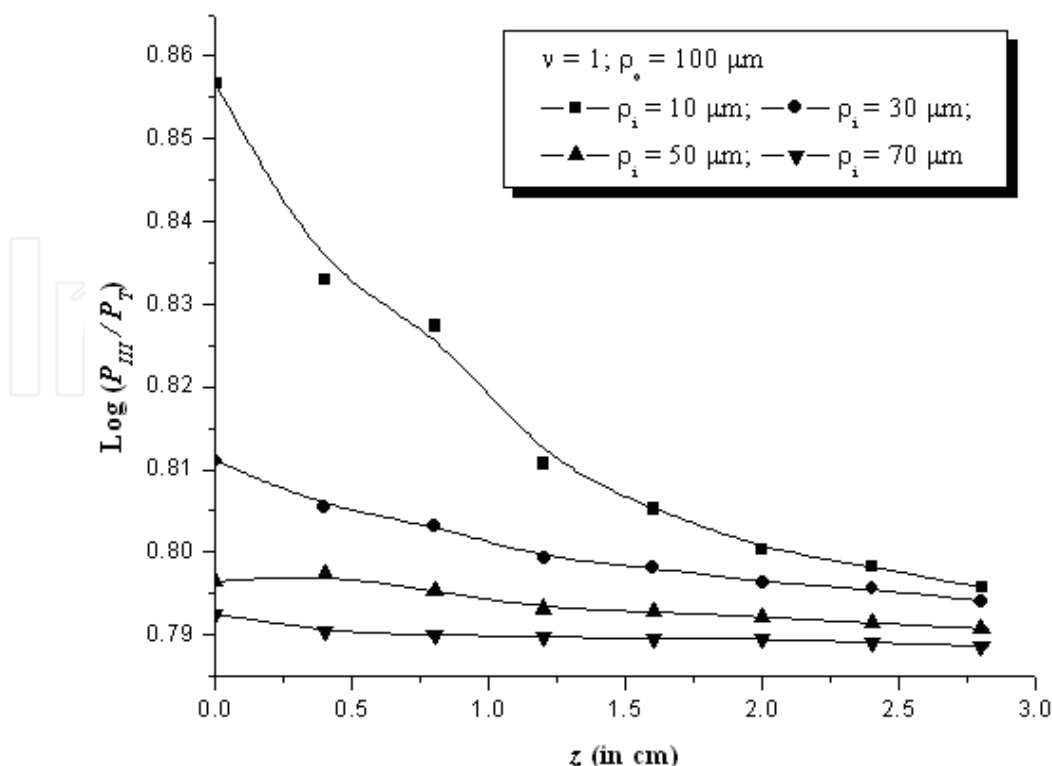


Fig. 22c. TE mode power confinement in the outermost clad of LCTOF.

Figs. 23a, 23b and 23c illustrate the logarithmic plots of the relative power distributions in the LCTOF core, the inner clad and the outermost liquid crystal clad, respectively, along the taper length. These figures present a comparative feature of the cases with different values of the azimuthal index. We consider two illustrative values (viz. $10 \mu\text{m}$ and $30 \mu\text{m}$) of the core radius of the input taper end, and the core output end radius is taken to be $100 \mu\text{m}$. We observe from fig. 23a that, for both the values of input core radius, the modes with higher azimuthal index ($\nu = 2$) transport a little higher amount of power as compared to that by the lower azimuthal index value ($\nu = 1$), and the difference increases as we move to look at the situations of power confinements in the inner and the outer clads. We notice from fig. 23c that the confinement remains maximum in the outermost liquid crystal clad, and also, the modes with $\nu = 2$ carry substantially large amount of power than those with $\nu = 1$.

The aforesaid discussions correspond to the situations when the TE modes are excited in an LCTOF. Now, considering the excitation of the TM modes, the logarithmic variations of the power confinement factor are illustrated in figs. 24 and 25 for the azimuthal index $\nu = 1$ and the tapered section length as 5 cm .

Fig. 24a corresponds to the power transmission through the LCTOF core when the different parameters are chosen similar to the case of TE modes, i.e. a fixed input end core radius as $60 \mu\text{m}$ and varying output end core radius as $80 \mu\text{m}$, $100 \mu\text{m}$, $120 \mu\text{m}$ and $140 \mu\text{m}$. We observe from fig. 24a that a relatively high amount of power is confined into the core as compared to the situation of TE modes (fig. 21a). Further, fig. 24b shows that the highest amount of power is found to be sustained in the inner clad, which is in contrast to the feature observed corresponding to the case of TE modes which presents the maximum amount of power to be confined in the outermost clad. In the present case, of TM mode

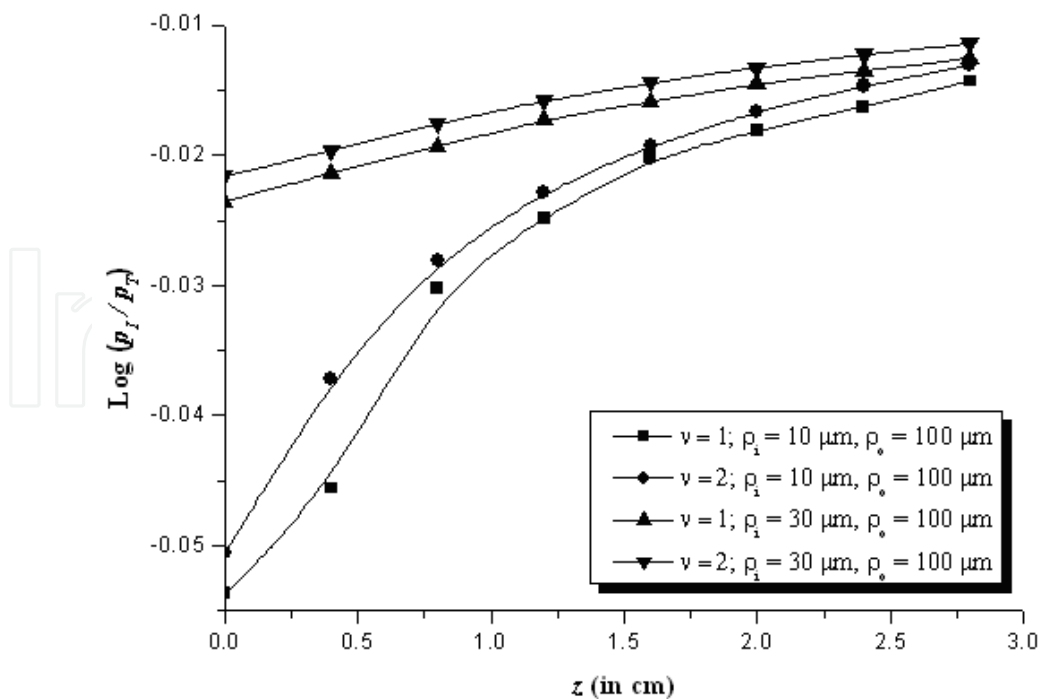


Fig. 23a. TE mode power distribution in the LCTOF core.

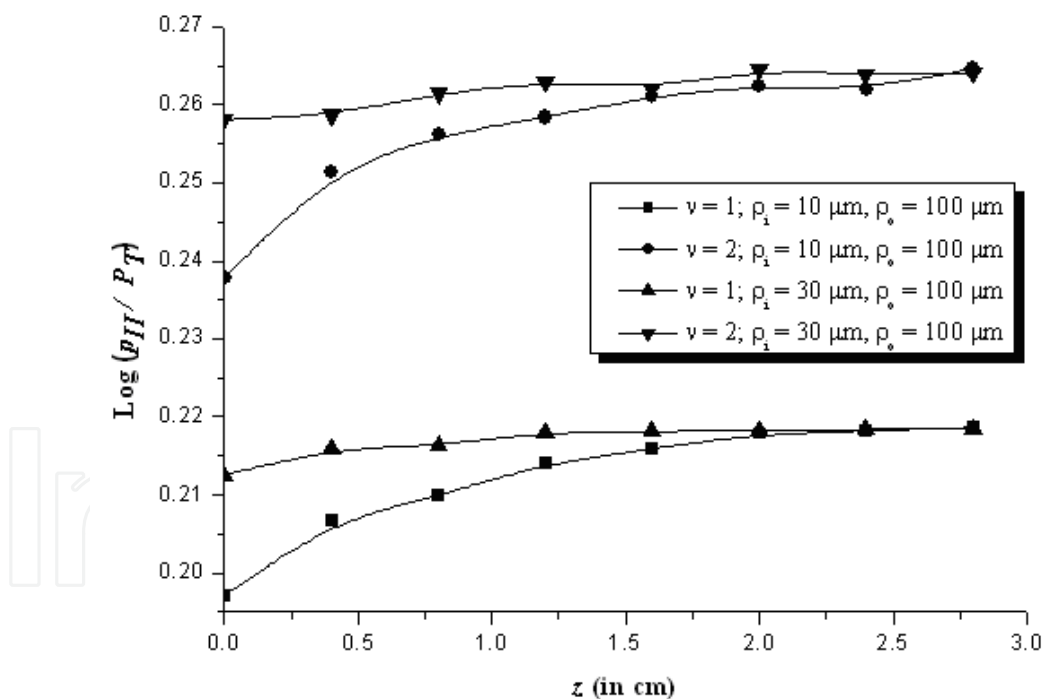


Fig. 23b. TE mode power distribution in the LCTOF inner clad.

excitation, we observe that the power confinement in the outermost liquid crystal clad (fig. 24c) is slightly less than that in the inner clad region.

We also observe that the trend of variation of the confinement factor in TM mode excitation seems to be opposite to that noticed corresponding to the case of TE modes. This is because, in figs. 24a and 24b, confinement falls with the increase in the taper length, and remains

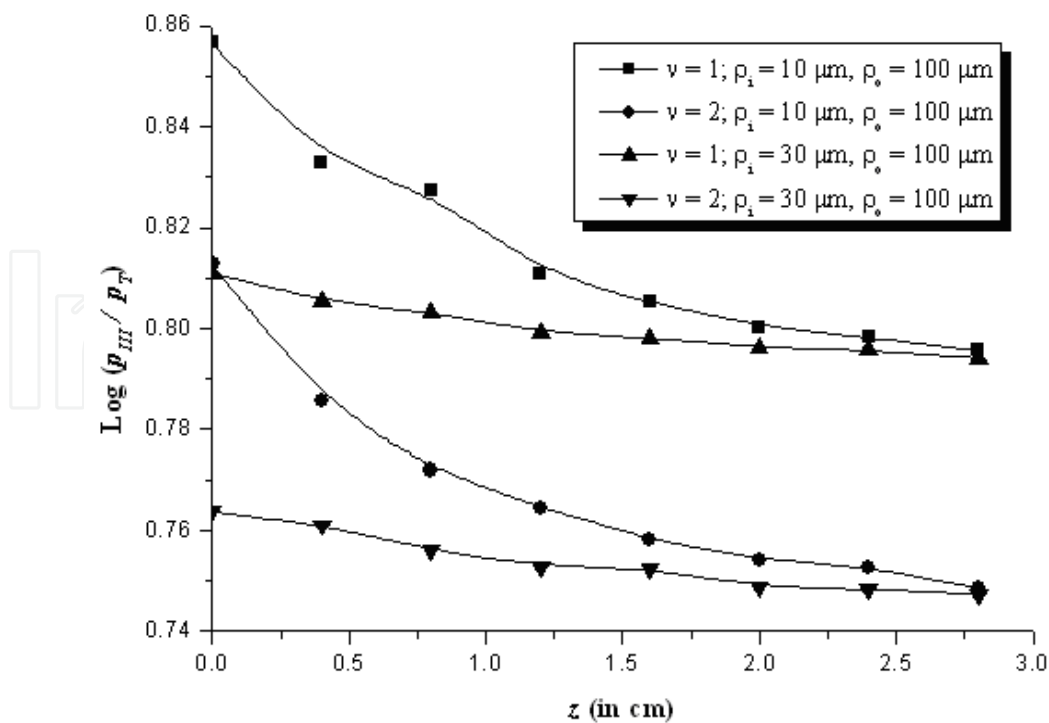


Fig. 23c. TE mode power distribution in the LCTOF outer clad.

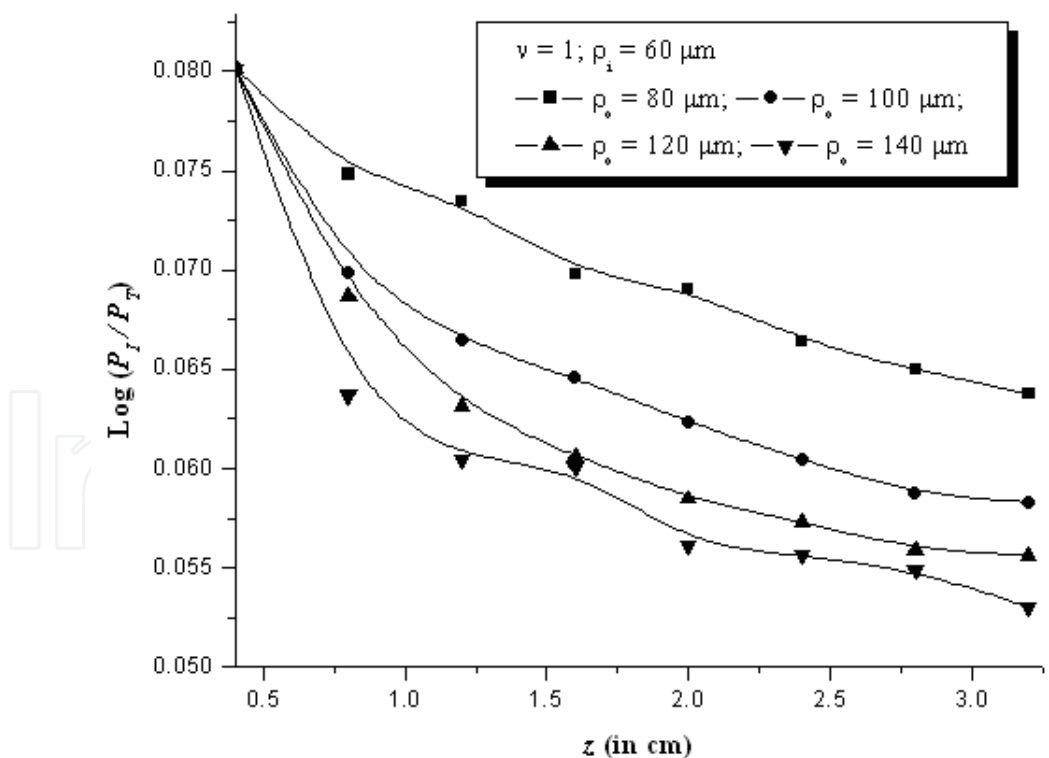


Fig. 24a. TM mode power confinement in LCTOF core.

minimum at the output end of the taper section. This is attributed to the TM mode properties whereby the power is gradually being coupled to the neighboring regions of the guide with increasing fiber dimensions.

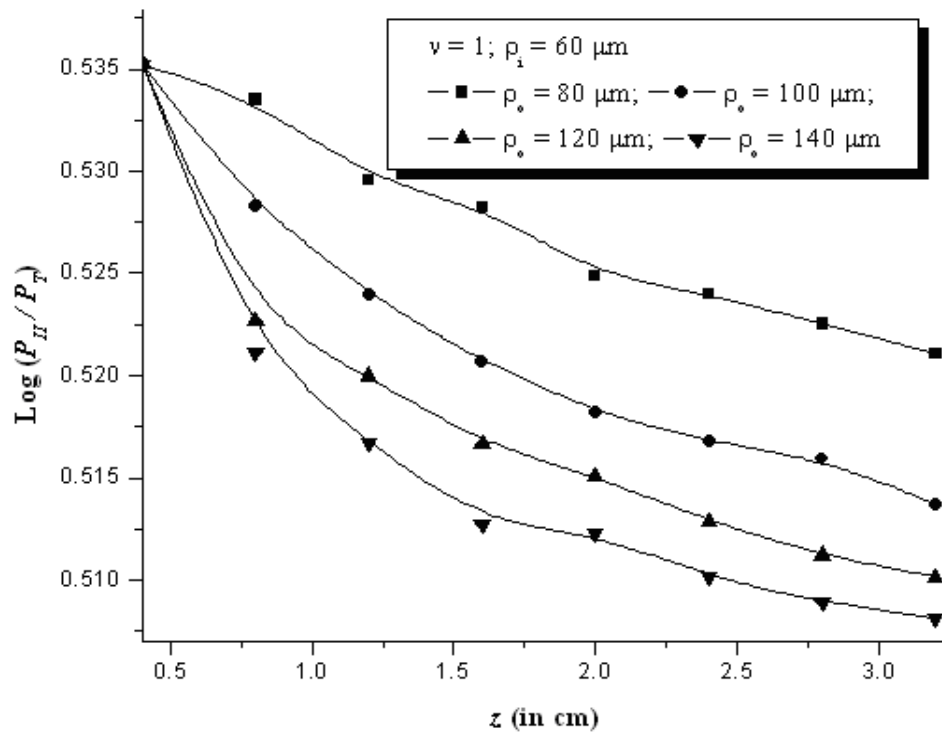


Fig. 24b. TM mode power confinement in the inner clad of LCTOF.

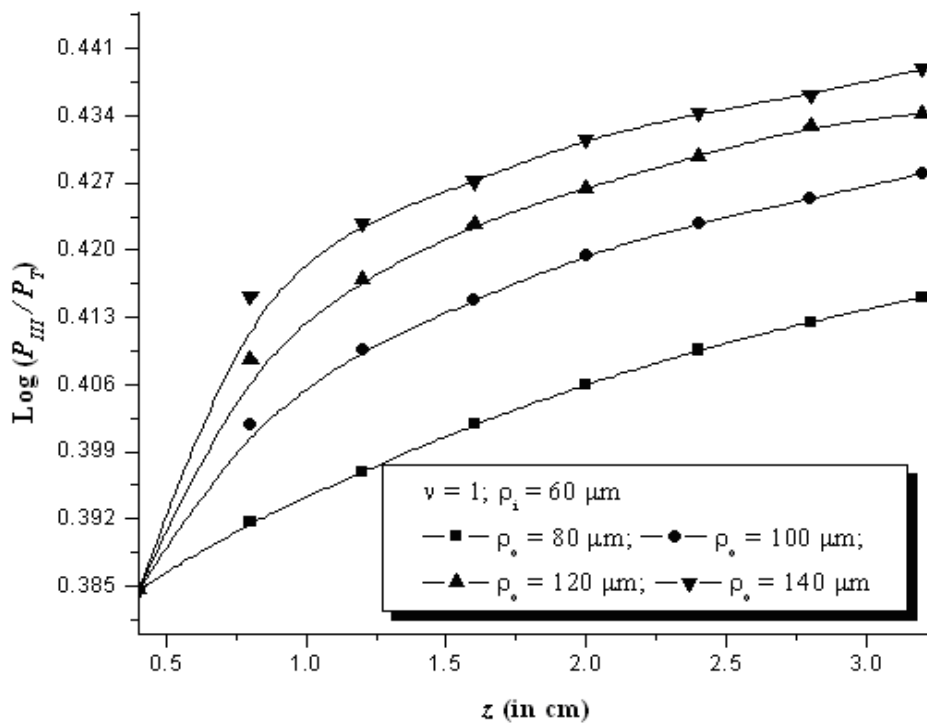


Fig. 24c. TM mode power confinement in the outermost clad of LCTOF.

Figs. 25 illustrate the logarithmic plots of power confinement in different fiber sections with fixed output end dimension of the taper section and varying size of the input end. Confinement in the fiber core is presented in fig. 25a, whereas those in the inner and the outer clads are illustrated in figs. 25b and 25c, respectively. We consider the output end

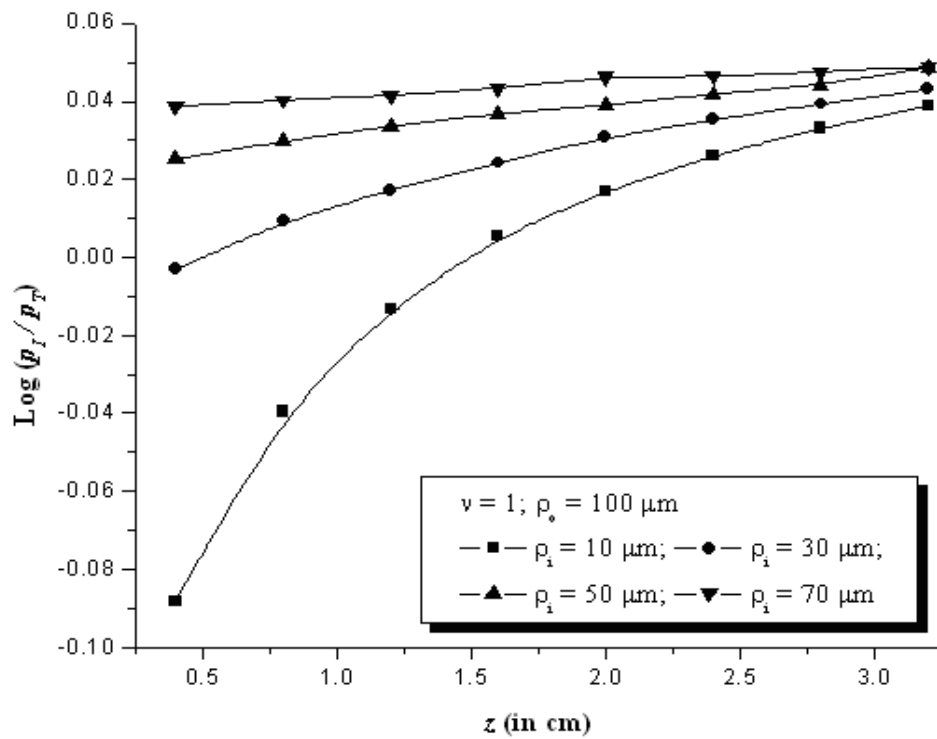


Fig. 25a. TM mode power confinement in LCTOF core.

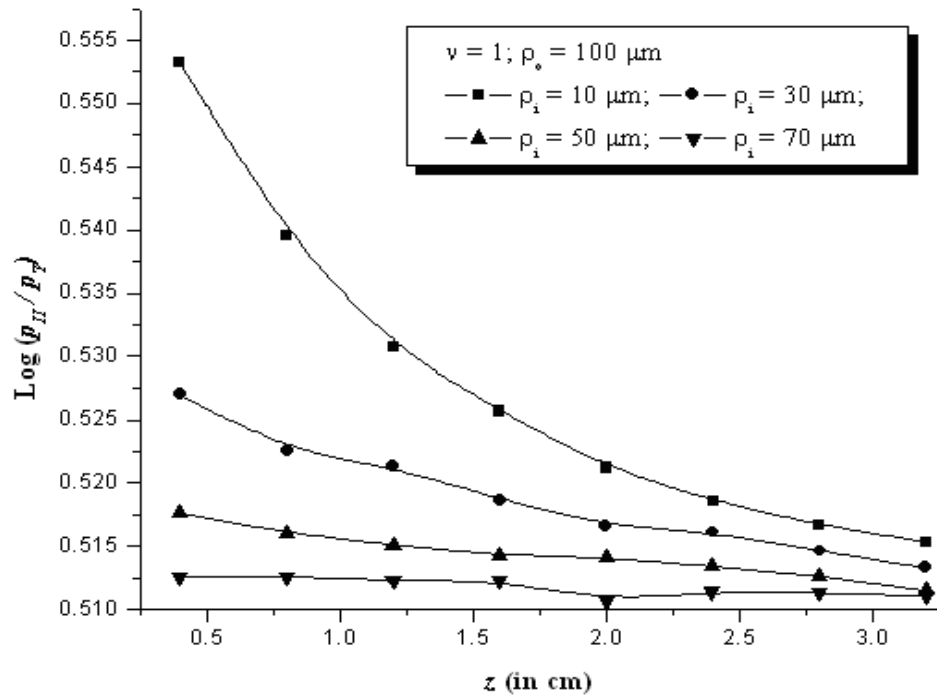


Fig. 25b. TM mode power confinement in the inner clad of LCTOF.

radius to be $100\ \mu\text{m}$ whereas the different input end radii are $10\ \mu\text{m}$, $30\ \mu\text{m}$, $50\ \mu\text{m}$ and $70\ \mu\text{m}$. We observe in these figures that the confinement remains strongest corresponding to the largest input end dimension, i.e. $70\ \mu\text{m}$ radius. Also, with such a fiber structure, the confinement remains most uniform too. This is attributed to the fact that the waves face maximum variations in respect of their boundaries with large difference in the output and

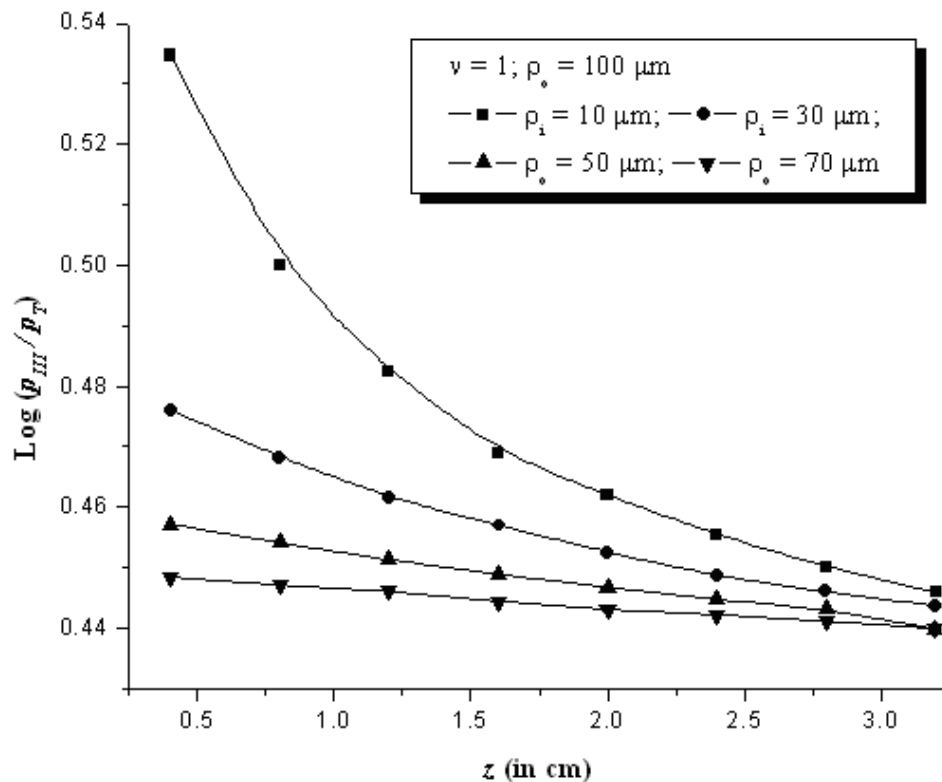


Fig. 25c. TM mode power confinement in the outermost clad of LCTOF.

the input end dimensions. However, the noticeable fact remains that the maximum amount of power is confined in the inner clad section, and the outermost clad sustains slightly less amount of power than the inner clad; the core section confines the minimum amount of power.

In order to have a comparative look at the power confinements by the modes with different azimuthal indices under the TM mode excitation, figs. 26a, 26b and 26c illustrate the logarithmic plots of the power confinement factor in the LCTOF core, the inner clad and the outermost liquid crystal clad, respectively, along the taper length. Once again, we use in our computations two illustrative values (viz. $10 \mu\text{m}$ and $30 \mu\text{m}$) of the core radius of the input taper end, and the core output end radius is taken to be fixed as $100 \mu\text{m}$. We observe from these figures that the modes with $\nu = 1$ and $\nu = 2$ transport almost similar amount of power in all the three LCTOF sections, which is unlike the situation observed in the case of the TE mode excitation where the modes with higher azimuthal index transmit substantially large amount of power than those with lower azimuthal index value.

It can thus be inferred that, in LCTOFs with radially anisotropic liquid crystal outermost clad, the TE modes transmit the maximum amount of power in the outermost section of the fiber. This feature is not that pronounced corresponding to the TM mode excitation as the confinement mostly remains in the inner clad section in this case. As stated before, the higher amount of power distribution in the outermost clad section can be interpreted as if the power is *leaking off* the LCTOF core, and transferred to the fiber clad. This feature is strongly observed in the case of TE mode excitation, and the phenomenon is attributed to the presence of radially anisotropic liquid crystal material in the outermost clad.

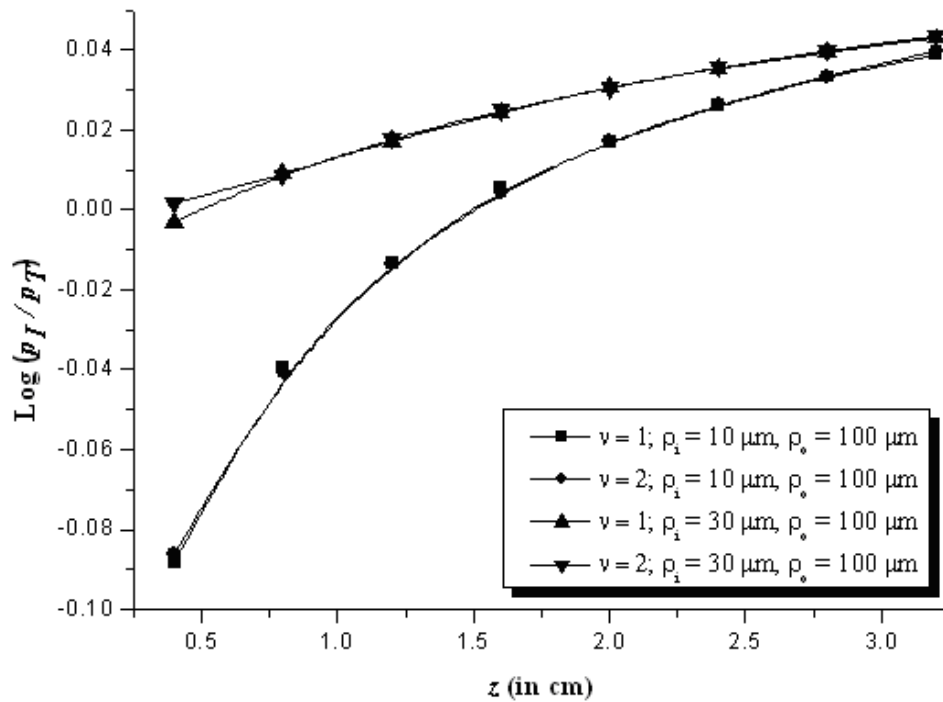


Fig. 26a. TM mode power distribution in LCTOF core.

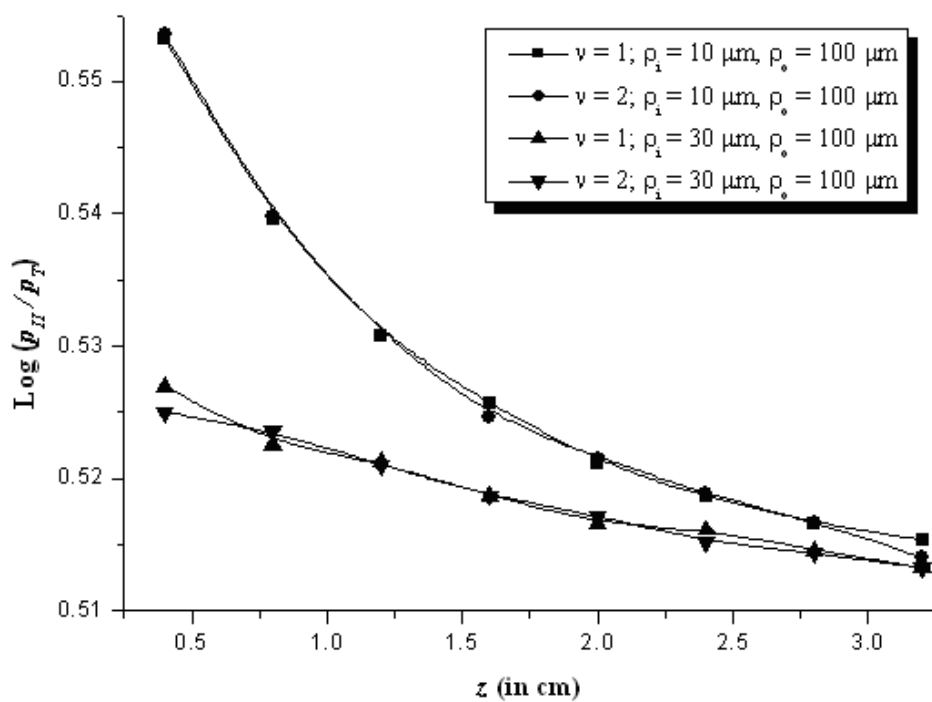


Fig. 26b. TM mode power distribution in LCTOF inner clad.

Apart from the material used in LCTOF fabrication, the taper structure of guide essentially plays a vital role to transfer power to the outermost clad. TOFs are already established in coupling applications, and the inclusion of liquid crystal section makes the structure more

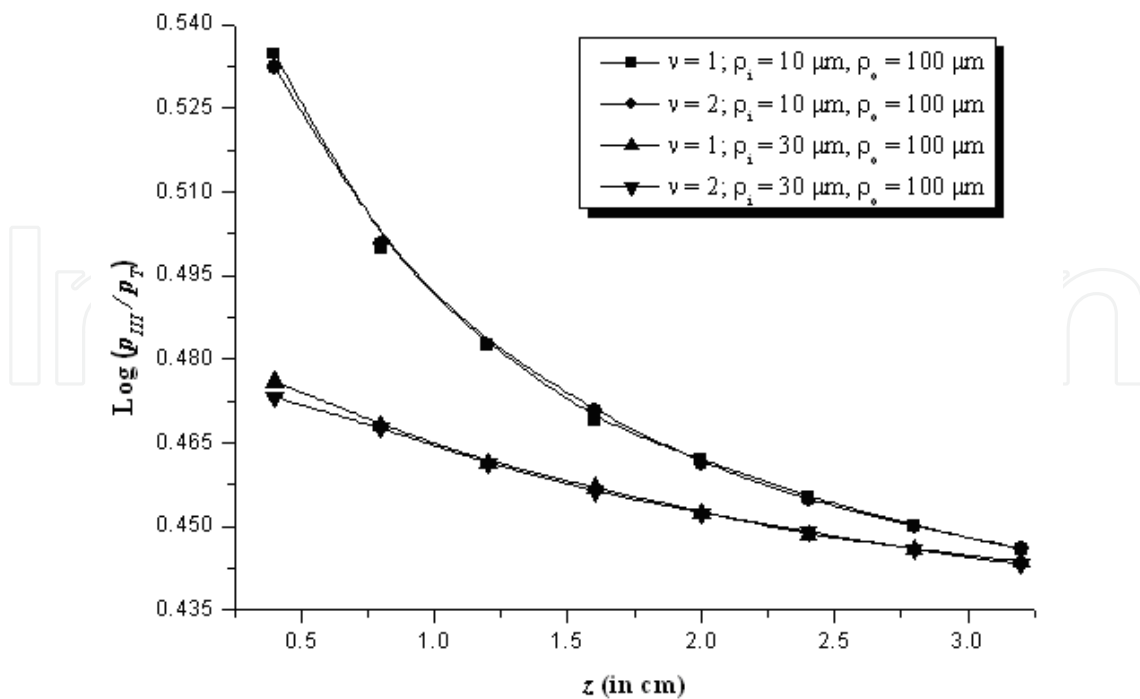


Fig. 26c. TM mode power distribution in LCTOF outer clad.

attractive for promising use. Thus, an amalgamation of the taper structure and the clad anisotropy brings in an enhanced confinement of power in the outermost clad section, and this feature opens up a demanding usefulness of LCTOFs in optical sensing and other coupling applications.

5. Conclusion

The article basically describes the EM wave propagation characteristics of TOFs considering various forms of them, viz. simple dielectric TOFs, dielectric TOFs with twists in the form of helical clad, and TOFs with radially anisotropic liquid crystal clad. The study of dielectric TOFs is presented under the assumption of a small variation of the core radius with the fiber length. The eigenvalue equations for such TOFs are developed, and the dispersion characteristics are described, which show almost similar features as that for conventional dielectric fibers. However, the study reveals that the tapered feature of fibers greatly affects the cutoff value of the normalized frequency parameter, and it is much reduced as compared to that exhibited by conventional fibers. The power transmission characteristics of such dielectric TOFs is also described in the form of the relative power distribution over the taper length considering the cases of meridional and the lowest skew modes. It is noticed that, in the case of meridional mode, the relative power exhibits some sort of linear dependence on the taper length. Corresponding to the skew mode, the power remains relatively uniform over the taper length, and the uniformity increases with the increase in the dimension of the taper output. The feature of uniform distribution of optical power in fibers remains much useful for communication purposes.

While dealing with the case of helical clad TOFs, the dispersion characteristics and the cutoff situations are deduced corresponding to two particular values of the helix pitch

angle – helical turns being parallel (i.e. 0°) and perpendicular (i.e. 90°) to the direction of wave propagation. It is found that the modes travel through the fiber with higher propagation constant under the situation when the helical turns are perpendicular to the optical axis than the case of parallel wraps. However, when the propagation features are compared with the situation of fibers without helical wraps, it is noticed that the helical turns possess the tendency to increase the modal propagation constants. This exhibits the importance of the helix pitch angle in controlling the propagation characteristics of such TOFs.

Study of LCTOFs with radially anisotropic liquid crystal clads is also touched upon, and the dispersion characteristics as well as the features of power transmission corresponding to the TE and TM mode excitations are reported. It is found that the TE eigenmodes propagate in the guide with larger propagation constants as compared to the TM ones. The results further reveal that, in the case of TE mode excitation, a large amount of power remains in the outermost liquid crystal region with substantial difference in the power sustained in the fiber core and the inner dielectric clad. The existence of a large amount of power in the outermost clad region is attributed to the presence of radially anisotropic liquid crystal medium used in the LCTOF. Further, the tapered structure of guide also plays the role for the proliferation of *power transfer* to the outermost clad. As such, a large amount of TE mode power in the outermost liquid crystal clad essentially indicates the prominent use of LCTOFs in optical sensing and/or coupling applications. At this point, it is noteworthy that TOFs are proved much promising for field coupling, and the incorporation of liquid crystal section makes them more demanding, as demonstrated through the results.

6. Acknowledgement

This work is partially supported by the Fundamental Research Grant Project (FRGS/1/2011/TK/UKM/01/16) sanctioned by the Ministry of Higher Education, Malaysia. The author is thankful to Prof. Burhanuddin Yeop Majlis for constant encouragement and help. He is also grateful to Prof. S. Shaari for some stimulating discussions and fruitful suggestions.

7. References

- [1] N. Engheta and P. Pelet, "Modes in chirowaveguides," *Opt. Lett.*, Vol. 14, 593–595, 1989.
- [2] H. Cory and I. Rosenhouse, "Electromagnetic wave propagation along a chiral slab," *IEE Proc. H*, Vol. 138, 51–54, 1991.
- [3] Kh.S. Singh, P.K. Choudhury, V. Misra, P. Khastgir, and S.P. Ojha, "Field cutoffs of three-layer parabolically deformed planar chirowaveguides," *J. Phys. Soc. Jpn.*, Vol. 62, 3778–3782, 1993.
- [4] P.K. Choudhury and T. Yoshino, "Dependence of optical power confinement on core/cladding chiralities in a simple chirofiber," *Microw. and Opt. Tech. Lett.*, Vol. 32, 359–364, 2002.
- [5] P.K. Choudhury and T. Yoshino, "TE and TM modes power transmission through liquid crystal optical fibers," *Optik*, Vol. 115, 49–56, 2004.

- [6] A. Nair and P.K. Choudhury, "On the analysis of field patterns in chirofibers," *J. Electromag. Waves and Appl.*, Vol. 21, 2277–2286, 2007.
- [7] A. Kumar, K. Thyagarajan, and A.K. Ghatak, "Analysis of rectangular core dielectric waveguides: an accurate perturbation approach," *Opt. Lett.*, Vol. 8, pp. 63–65, 1983.
- [8] P.K. Choudhury, P. Khastgir, and S.P. Ojha, "Analysis of the guidance of electromagnetic waves by a deformed planar waveguide with parabolic cylindrical boundaries," *J. Appl. Phys.*, Vol. 71, pp. 5685–5688, 1992.
- [9] P.K. Choudhury, P. Khastgir, S.P. Ojha, and K.S. Ramesh, "An exact analytical treatment of parabolically deformed planar waveguides near cutoff," *Optik*, Vol. 95, pp. 147–151, 1994.
- [10] P.K. Shukla, P.K. Choudhury, P. Khastgir, and S.P. Ojha, "Comparative aspects of a metal-loaded triangular waveguide with uniform and non-uniform distribution of Goell's matching points," *J. Inst. Electron. Telecommun. Eng.*, Vol. 41, pp. 217–220, 1995.
- [11] P.K. Choudhury, "On the preliminary study of a dielectric guide having a Piet Hein geometry," *Ind. J. Phys.*, Vol. 71B, pp. 191–196, 1997.
- [12] P. Sharan, S.P. Ojha, P. Khastgir, and P.K. Choudhury, "Modal cutoff of an optical waveguide having a lemniscate of Bernoulli-type core cross-section," *Microw. and Opt. Tech. Lett.*, Vol. 14, pp. 170–172, 1997.
- [13] P.K. Choudhury and O.N. Singh, "Some multilayered and other unconventional lightguides," In: *Electromagnetic fields in unconventional structures and materials* (O.N. Singh and A. Lakhtakia, Eds.), John Wiley: New York, pp. 289–357, 2000.
- [14] D.T. Cassidy, D.C. Johnson, and K.O. Hill, "Wavelength-dependent transmission of monomode optical fiber taper," *Appl. Opt.*, Vol. 24, pp. 945–950, 1985.
- [15] R.P. Payne, C.D. Hussey, and M.S. Yataki, "Modeling fused single-mode-fiber couplers," *Electron. Lett.*, Vol. 21, pp. 461–462, 1985.
- [16] A.C. Boucouvalas and G. Georgiou, "Biconical taper coaxial optical fiber couplers," *Electron. Lett.*, Vol. 21, pp. 864–865, 1985.
- [17] J.V. Wright, "Variational analysis of fused tapered couplers," *Electron. Lett.*, Vol. 21, pp. 1064–1065, 1985.
- [18] S. Lacroix, F. Gonthier, and J. Bures, "All-fiber wavelength filter from successive biconical tapers," *Opt. Lett.*, Vol. 11, pp. 671–673, 1986.
- [19] F. Gonthier, J. Lapierre, C. Veilleux, S. Lacroix, and J. Bures, "Investigation of power oscillations along tapered monomode fibers," *Appl. Opt.*, Vol. 26, pp. 444–449, 1987.
- [20] S. Lacroix, R. Bourbouriars, F. Gonthier, and J. Bures, "Tapered monomode optical fibers: understanding large power transfer," *Appl. Opt.*, Vol. 26, pp. 4421–4425, 1987.
- [21] H.S. Monteiro, R. Arradi, D.C. Dini, S.L.A. Carrara, and E. Conforti, "A spot reflection alignment system for fabrication of polarization-maintaining optical fiber couplers," *Microw. and Opt. Tech. Lett.*, Vol. 19, pp. 75–77, 1988.
- [22] R.J. Black, F. Gonthier, S. Lacroix, J. Lapierre, and J. Bures, "Tapered fibers: an overview," *Proc. SPIE*, Vol. 839, pp. 2–19, 1988.

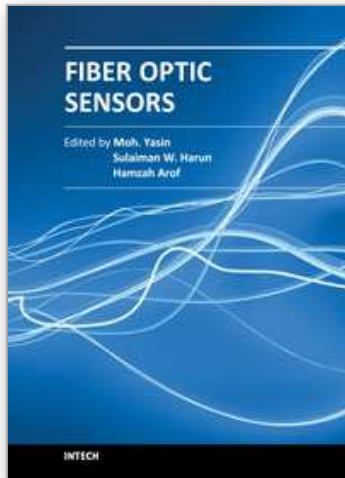
- [23] W.-C. Chang, S.-J. Chan, H.-C. Hou, and C.-Y. Sue, "Measurement of coupling coefficients of Ni:LiNbO directional couplers," *Microw. and Opt. Tech. Lett.*, Vol. 19, pp. 24–27, 1988.
- [24] M.C. Gabriel and N.O. Whittaker, "Measurement of optical waveguide coupling coefficients using multiple waveguide systems," *J. Light. Tech.*, Vol. 7, pp. 1343–1350, 1989.
- [25] A. Bolle and L. Lundgren, "Analytical solution of the field in a fiber up-taper with a parabolic index profile," *IEE Proc. J.: Optoelectron.*, Vol. 137, pp. 301–304, 1990.
- [26] K. Ono and H. Osawa, "Excitation characteristics of fundamental mode in tapered slab waveguides with nonlinear cladding," *Electron. Lett.*, Vol. 27, pp. 664–666, 1991.
- [27] K. Ono, S. Tsuruta, T. Sakai, H. Osawa, and Y. Okamoto, "Highly efficient coupling between two planar waveguides with different refractive index profiles by using nonlinear cladding," *IEEE Phot. Tech. Lett.*, Vol. 4, pp. 381–384, 1992.
- [28] A.K. Singh, P. Khastgir, O.N. Singh, and S.P. Ojha, "Local field configuration modes in a weakly guiding optical fiber with a conically annular core: an analytical study," *Jpn. J. Appl. Phys.*, Vol. 32, pp. L71–L74, 1993.
- [29] D.B. Singh, P. Khastgir, U.K. Singh, and O.N. Singh, "Modal analysis of a dielectric waveguide with planar guiding-nonguiding boundaries with a flare in the direction of propagation," *Microw. and Opt. Tech. Lett.*, Vol. 17, pp. 394–398, 1998.
- [30] D.B. Singh, P. Khastgir, U.K. Singh, and O.N. Singh, "Unattenuated global modes in a planar dielectric waveguide with a flare in the direction of propagation," *Microw. and Opt. Tech. Lett.*, Vol. 19, pp. 77–80, 1998.
- [31] A.R. Nelson, "Coupling in optical waveguides by tapers," *Appl. Opt.*, Vol. 14, pp. 3012–3015, 1975.
- [32] M.G.F. Wilson and G.A. The, "Tapered optical directional couplers," *IEEE Trans. Microw. Theory Tech.*, Vol. MTT-23, pp. 85–92, 1975.
- [33] T.K. Lin and J.P. Marton, "An analysis of optical waveguide tapers," *J. Appl. Phys.*, Vol. 18, pp. 53–62, 1979.
- [34] R.J. Black, F. Gonthier, S. Lacroix, and J.D. Love, "Tapered single-mode fibres and devices: I. adiabaticity criteria," *IEE Proc. -J*, Vol. 138, pp. 343–354, 1991.
- [35] J.R. Pierce, *Traveling wave tubes*, D. Van Nostrand, New Jersey, 1950.
- [36] U.N. Singh, O.N. Singh II, P. Khastgir, and K.K. Dey, "Dispersion characteristics of a helically clad step-index optical fiber: an analytical study," *J. Opt. Soc. Am. B*, Vol. 12, pp. 1273–1278, 1995.
- [37] C. Veilleux, J. Lapierre, and J. Bures, "Liquid-crystal-clad tapered fibers," *Opt. Lett.*, Vol. 11, pp. 733–735, 1986.
- [38] M. Green and S.J. Madden, "Low loss nematic liquid crystal cored fiber waveguides," *Appl. Opt.*, Vol. 28, pp. 5202–5203, 1989.
- [39] H. Lin, P.P. Muhoray, and M.A. Lee, "Liquid crystalline cores for optical fibers," *Mol. Cryst. Liq. Cryst.*, Vol. 204, pp. 189–200, 1991.
- [40] S.-T. Wu and U. Efron, "Optical properties of thin nematic liquid crystal cells," *Appl. Phys. Lett.*, Vol. 48, pp. 624–636, 1986.

- [41] N. Amitay and H.M. Presby, "Optical fiber up-tapers modeling and performance analysis," *J. Light. Tech.*, Vol. 7, pp. 131–137, 1989.
- [42] M. Abramowitz and I.A. Stegun, *Handbook of mathematical functions*, New York: Dover; 1965.
- [43] M.H. Lim, S.C. Yeow, P.K. Choudhury, and D. Kumar, "Towards the dispersion characteristics of tapered core dielectric optical fibers," *J. Electromagn. Waves and Appl.*, Vol. 20, 1597–1609, 2006.
- [44] D. Gloge, "Weakly guiding fibers," *Appl. Opt.*, Vol. 10, pp. 2252–2258, 1971.
- [45] P.K. Choudhury and T. Yoshino, "A rigorous analysis of the power distribution in plastic clad annular core optical fibers," *Optik*, Vol. 113, pp. 481–488, 2002.
- [46] A.H. Cherin, *An introduction to optical fibers*, McGraw-Hill, New York, 1987.
- [47] S.C. Yeow, M.H. Lim, and P. K. Choudhury, "A rigorous analysis of the distribution of power in plastic clad linear tapered fibers," *Optik*, Vol. 117, 405–410, 2006.
- [48] D. Kumar and O.N. Singh II, "Some special cases of propagation characteristics of an elliptical step-index fiber with a conducting helical winding on the core-cladding boundary – an analytical treatment," *Optik*, Vol. 112, pp. 561–566, 2000.
- [49] D. Kumar and O.N. Singh II, "An analytical study of the modal characteristics of annular step-index waveguide of elliptical cross-section with two conducting helical windings on the two boundary surfaces between the guiding and the non-guiding regions," *Optik*, Vol. 113, pp. 193–196, 2002.
- [50] D. Kumar and O.N. Singh II, "Modal characteristic equation and dispersion curves for an elliptical step-index fiber with a conducting helical winding on the core-cladding boundary – an analytical study," *J. Light. Tech.*, Vol. 20, pp. 1416–1424, 2002.
- [51] D. Kumar, P.K. Choudhury, and F.A. Rahman, "Towards the characteristic dispersion relation for step-index hyperbolic waveguide with conducting helical winding," *Prog. in Electromagn. Res.*, Vol. PIER 71, pp. 251–275, 2007.
- [52] D. Kumar, P.K. Choudhury, and O.N. Singh II, "Towards the dispersion relations for dielectric optical fibers with helical windings under slow- and fast-wave considerations – a comparative analysis," *Prog. in Electromagn. Res.*, Vol. PIER 80, pp. 409–420, 2008.
- [53] A.H.B.M. Safie and P.K. Choudhury, "On the field patterns of helical clad dielectric optical fibers," *Prog. in Electromagn. Res.*, Vol. PIER 91, 69–84, 2009.
- [54] P. K. Choudhury and D. Kumar, "On the slow-wave helical clad elliptical fibers," *J. Electromagn. Waves and Appl.*, Vol. 24, pp. 1931–1942, 2010.
- [55] D.A. Watkins, *Topics in electromagnetic theory*, Wiley, USA, 1958.
- [56] C.C. Siong and P.K. Choudhury, "Propagation characteristics of tapered core helical clad dielectric optical fibers," *J. Electromagn. Waves and Appl.*, Vol. 23, pp. 663–674, 2009.
- [57] P.K. Choudhury and P.T.S. Ping, "On the dispersion relations of tapered core optical fibers with liquid crystal clad," *Prog. in Electromagn. Res.*, Vol. PIER 118, pp. 117–133, 2011.
- [58] P.K. Choudhury and W.K. Soon, "On the tapered optical fibers with radially anisotropic liquid crystal clad," *Prog. in Electromagn. Res.*, Vol. PIER 115, pp. 461–475, 2011.

- [59] P.K. Choudhury and W.K. Soon, On the transmission by liquid crystal tapered optical fibers," *Optik*, Vol. 122, pp. 1061–1068, 2011.

IntechOpen

IntechOpen



Fiber Optic Sensors

Edited by Dr Moh. Yasin

ISBN 978-953-307-922-6

Hard cover, 518 pages

Publisher InTech

Published online 22, February, 2012

Published in print edition February, 2012

This book presents a comprehensive account of recent advances and researches in fiber optic sensor technology. It consists of 21 chapters encompassing the recent progress in the subject, basic principles of various sensor types, their applications in structural health monitoring and the measurement of various physical, chemical and biological parameters. It also highlights the development of fiber optic sensors, their applications by providing various new methods for sensing and systems, and describing recent developments in fiber Bragg grating, tapered optical fiber, polymer optical fiber, long period fiber grating, reflectometry and interferometry based sensors. Edited by three scientists with a wide knowledge of the field and the community, the book brings together leading academics and practitioners in a comprehensive and incisive treatment of the subject. This is an essential reference for researchers working and teaching in optical fiber sensor technology, and for industrial users who need to be aware of current developments and new areas in optical fiber sensor devices.

How to reference

In order to correctly reference this scholarly work, feel free to copy and paste the following:

P. K. Choudhury (2012). Tapered Optical Fibers – An Investigative Approach to the Helical and Liquid Crystal Types, Fiber Optic Sensors, Dr Moh. Yasin (Ed.), ISBN: 978-953-307-922-6, InTech, Available from: <http://www.intechopen.com/books/fiber-optic-sensors/tapered-optical-fibers-an-investigative-approach-to-the-helical-and-liquid-crystal-types>

INTECH
open science | open minds

InTech Europe

University Campus STeP Ri
Slavka Krautzeka 83/A
51000 Rijeka, Croatia
Phone: +385 (51) 770 447
Fax: +385 (51) 686 166
www.intechopen.com

InTech China

Unit 405, Office Block, Hotel Equatorial Shanghai
No.65, Yan An Road (West), Shanghai, 200040, China
中国上海市延安西路65号上海国际贵都大饭店办公楼405单元
Phone: +86-21-62489820
Fax: +86-21-62489821

© 2012 The Author(s). Licensee IntechOpen. This is an open access article distributed under the terms of the [Creative Commons Attribution 3.0 License](#), which permits unrestricted use, distribution, and reproduction in any medium, provided the original work is properly cited.

IntechOpen

IntechOpen